Tin-based "super-POSS" building blocks in epoxy nanocomposites with highly improved oxidation resistance

Adam Strachota, Krzysztof Rodzen, François Ribot, Magdalena Perchacz, Miroslava Trchova, Milos Steinhart, Larisa Starovoytova, Miroslav Slouf, Beata Strachota

Tin-based "super-POSS" building blocks in epoxy nanocomposites with highly improved oxidation resistance

Adam Strachota [a, *], Krzysztof Rodzeń [a], François Ribot [b, c, d], Magdalena Perchacz [a], Miroslava Trchová [a], Miloš Steinhart [a], Larisa Starovoytova [a], Miroslav Šlouf [a], Beata Strachota [a]

[a] *Institute of Macromolecular Chemistry v.v.i., Academy of Sciences of the Czech Republic, Heyrovskeho nam. 2, CZ-162 00 Praha, Czech Republic*
[b] *Sorbonne Universités, UPMC Univ Paris 06, UMR 7574, Chimie de la Matière Condensée de Paris, F-75005 Paris, France*
[c] *CNRS, UMR 7574, Chimie de la Matière Condensée de Paris, F-75005 Paris, France*
[d] *Collège de France, UMR 7574, Chimie de la Matière Condensée de Paris, F-75005 Paris, France*

A novel tin-based POSS analogue, butylstannoxane dodecamer, was incorporated as chemically active nanofiller in epoxy resins and achieved a considerable anti-oxidative activity already near 0.05 wt% and very high activity near 1 wt%. The amino-functional nanofiller, which bonds as a linear segment, displayed a high reactivity towards the resin components during cure and was very poorly extractable. Interestingly, at elevated temperatures, the stannoxane nanofiller, whose functional substituents are attached by ionic bonds, displays a considerable short-range mobility in the matrix, and in course of a nano-phase-separation process, rearranges and polymerizes to needle-like nano-domains. This effect leads to additional crosslinking in the nanocomposite. This "solid-phase nano-precipitation" does not occur under oxidative conditions, where the nanofiller preferentially undergoes crosslinking with matrix chains and is thereby immobilized. Nanocomposite synthesis, characterization and the concentration dependence of the nanofiller effect are presented.

1. Introduction

A tin-based heavy analogue (Scheme 1) of the well-known polyhedral oligomeric silsesquioxane (POSS) nano-building block (Scheme 2) was incorporated into epoxy nanocomposites as chemically reactive filler with a strong anti-oxidative effect, which was investigated and optimized in this work. A general advantage of nanocomposites in comparison with conventional ones consists in the small size of filler, which mostly makes possible the use of the same processing techniques for the nanocomposites, like for the neat matrix [1–3]. In case that the filler is sufficiently small in comparison to visible light wavelength, optical transparency is also preserved. Additionally, the intrinsic properties of the selected nanofiller can provide specific chemical [4–6], optical [7–9], electrical [10,11], magnetic [12,13] or gas barrier [14–18] properties to the final nanocomposites. A marked mechanical reinforcement can be achieved with small nanofiller amounts, due to their high specific surface [19–23].

In their recent work, the authors investigated epoxy-nanocomposites reinforced by chemically bonded inorganic POSS cages [24–26] and demonstrated the key importance of POSS-POSS interactions for the mechanical reinforcement in these nanocomposites. The organic substituents attached onto the POSS surface were shown to control the filler–filler interaction [25]. The physical crosslinking and the topological constraint to elastic chain motion caused by hard domains of aggregated (matrix-bonded) POSS nanofiller was demonstrated [26,27] to contribute to mechanical reinforcement as well as to increased thermal stability.

The tin-based "super-POSS" (oligomeric butylstannoxane) shown in Scheme 1 is of interest due to its larger and heavier inorganic core, and also to its expected higher chemical reactivity in comparison to POSS, due to the stronger metallic character of Sn, and to the weaker Sn–C bond strength. The butylstannoxane dodecamer cage has an 1.2 nm long and 0.7 nm wide ellipsoid (polyhedral) inorganic core, which is covered by substituents, thereby achieving the overall dimensions of 2.3 × 4.7 nm [28],

* Corresponding author. Institute of Macromolecular Chemistry v.v.i., Academy of Sciences of the Czech Republic, Heyrovskeho nam. 2, CZ-162 00 Praha, Czech Republic. Tel.: +420 296 809 384.
E-mail address: strachota@imc.cas.cz (A. Strachota).

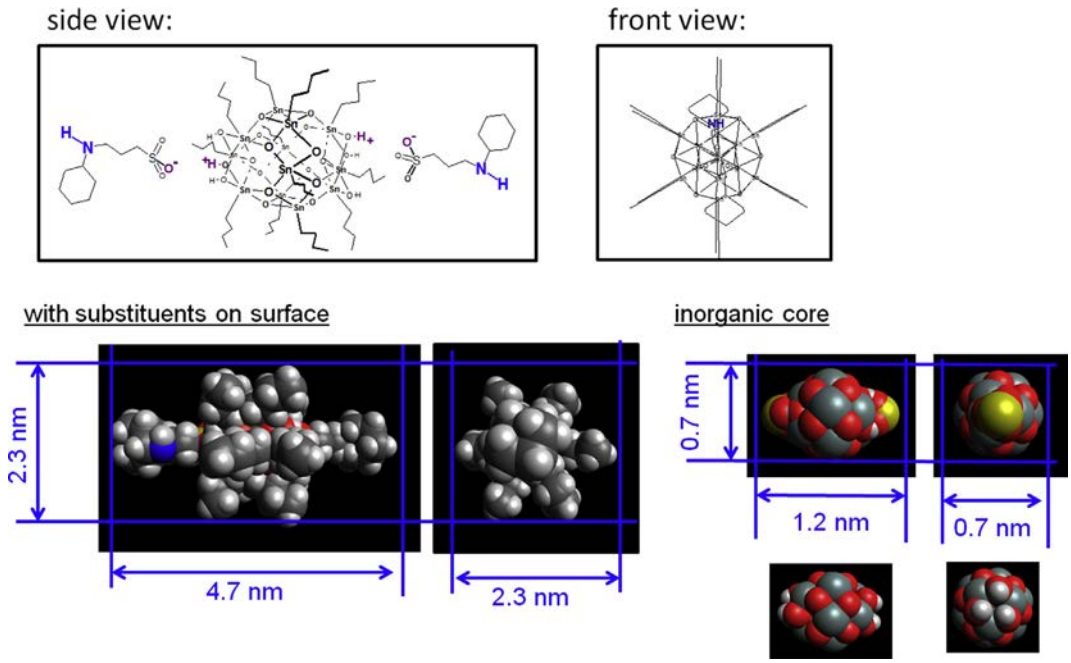

Scheme 1. Ellipsoid butylstannoxane dodecamer nano-building block used in this work: $[(nC_4H_9{-}Sn)_{12}(O)_{14}(OH)_6][O_3S{-}(CH_2)_3{-}NH{-}C_6H_{11}]_2$.

while the quasi-spherical POSS has the dimensions of 0.5 nm (core) and 1.5 nm core with typical substituents (Scheme 2). The attachment of two functional (or eventually inert) substituents by ionic bonds in axial positions of the stannoxane ellipsoid is a unique feature of this nanofiller, which makes possible its easy incorporation in polymer backbones and other linear structures [37,38]. In contrast to this, POSS can be easily obtained either monofunctional or octa-functional. Ionic dissociation of the stannoxane axial substituents, anion exchange reactions as well as supramolecular assembly under specific conditions were reported by Ribot et al. [29,30] and contribute to this nanofiller's unusual chemistry. A specific property is also the rearrangement into larger structures at elevated temperature, as reported by Ribot et al. [28].

Well-defined oligomeric alkylstannoxane cages similar to the one shown in Scheme 1 were first prepared in 1989 (POSS already in 1946) by Puff and Reuter [31], followed by Dakternieks [32]. In some analogy to siloxane chemistry, a large family of stannoxane compounds exists [33–35], including structures like linear, branched and ladder polymers, networks, drums and cages of different sizes. In 2000, Ribot [28,36], one of the authors of this work, developed a new, high-yield synthesis route (Scheme 3) to the butylstannoxane dodecamer, thus making possible its synthesis on a large scale, and its thorough characterization.

Only a few pioneering works were published up to date about polymeric materials containing stannoxane cages: Ribot et al. reported the preparation of carboxylate-based self-assembled organic-inorganic hybrids with stannoxane [37,38] and of a methacrylate-stannoxane copolymer [39]. Recently, also the authors of this work turned their interest to the heavier tin-based POSS analogue and incorporated oligomeric butylstannoxane for the first time into epoxy resins [40]. The stannoxane nanocomposites were shown to display some similar behaviour like the previously studied epoxy-POSS systems but they also displayed new properties like the anti-oxidative action of the nanofiller at moderately high concentrations (7 wt%). The nanofiller oligomerization was also observed, but surprisingly, the reaction practically

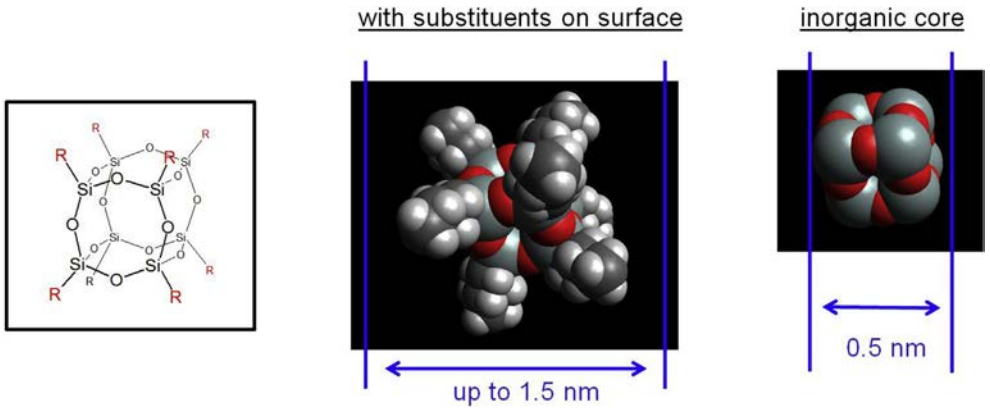

Scheme 2. Polyhedral oligomeric silsesquioxane (POSS) nano-building block.

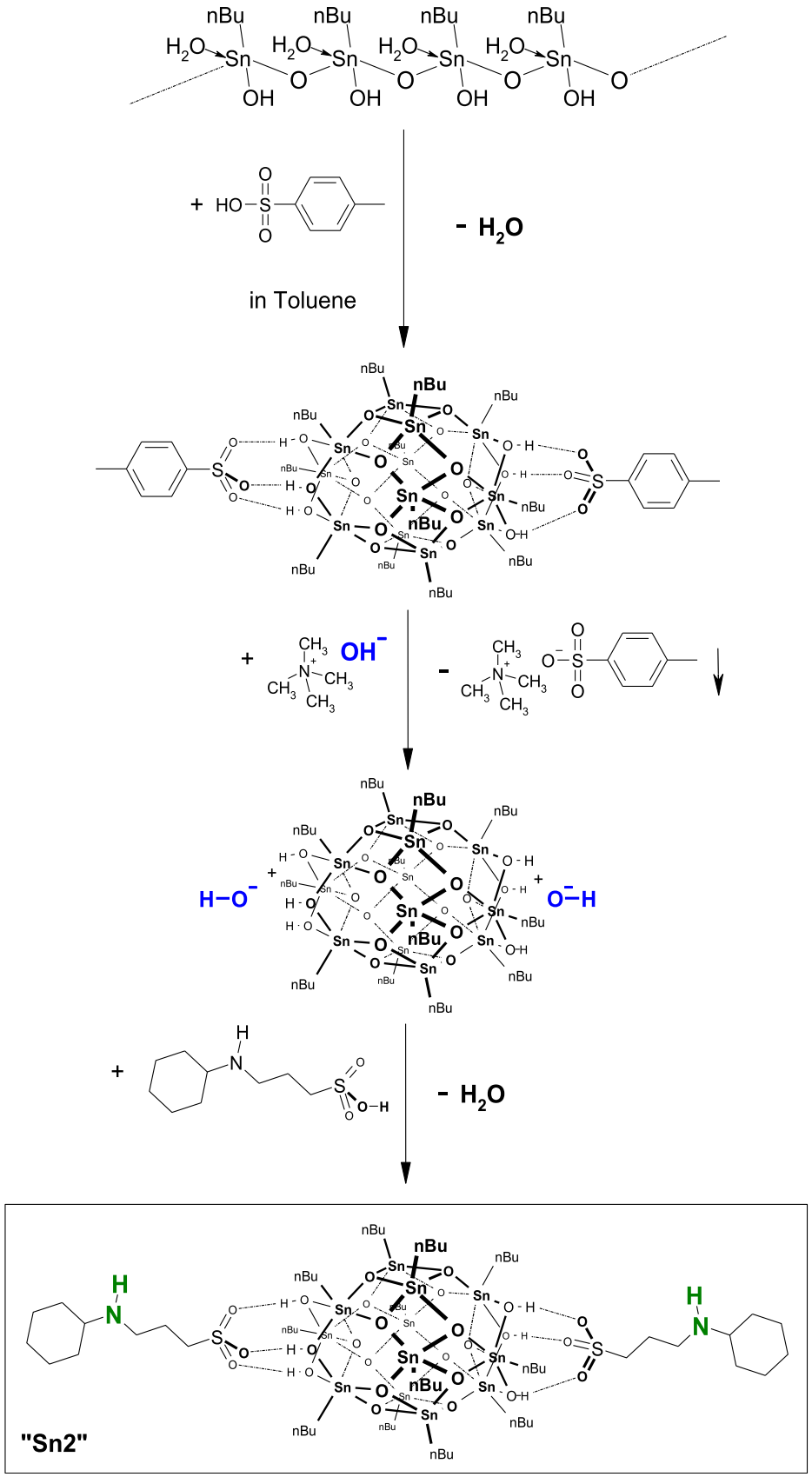

Scheme 3. Synthesis of the n-butylstannoxane dodecamer with N-cyclohexylamino end groups, which is incorporated as a linear unit in epoxy resins.

did not reinforce the composite, due to its complex morphology [40]. The above stannoxane nanofiller displayed a low reactivity (aromatic amine) towards the matrix's epoxy component and it was incorporated in the later stages of the matrix formation as a branching unit. This behaviour contributed to the complex morphology of the resulting nanocomposite, which in turn limited the anti-oxidative effect of the nanofiller.

The aim of this work was to fill epoxy matrices with a highly reactive stannoxane nanofiller (with aliphatic amino groups) which would be additionally bonded as a linear unit, and hence disperse monomolecularly, or at least form only simpler aggregates. Such a nanofiller would be more segmentally mobile and accessible for anti-oxidative reactions, as well as to the formation of new efficient crosslinks via stannoxane oligomerization. These expectations were fully met by the prepared nanocomposites, and a distinct anti-oxidizing effect was achieved already at very low concentrations.

2. Experimental

2.1. Materials

The poly(oxypropylene) diamines "Jeffamine D2000" (*molecular weight* = 1968 g/mol) and "Jeffamine D230" (*molecular weight* = 230 g/mol), the epoxides Diglycidylether of Bisphenol A ("DGEBA", 99.7% pure) and Phenyl glycidyl ether (PGE) as well as 1-Methylnaphthalene were purchased from Sigma–Aldrich.

The amino-functional Stannoxane cage "Sn2" was synthesized as described in the previous work of one of the authors [28,36], according to Scheme 3. Butyltin oxide hydroxide hydrate, BuSnO(OH).H_2O, was used as starting material and reacted with toluenesulfonic acid to yield the non-functional cage "Sn_0". The toluenesulfonate was converted into the dihydroxide in an ion exchange reaction using tetramethylammonium hydroxide. The dihydroxide was subsequently neutralized with N-cyclohexyl-3-aminopropanesulfonic acid, thus yielding "Sn2". All the above mentioned chemicals were purchased from Sigma–Aldrich.

2.2. Nanocomposite synthesis

2.2.1. Preparation of normally cured samples

The desired amounts of molten and supercooled epoxide DGEBA, of the liquid Jeffamine D2000, and of a 50 wt% stannoxane cage solution in toluene were mixed, the homogeneous clear reaction mixture was heated to 120 °C and stirred in an open vessel till gelation (typically ca. 40 min). Subsequently, the remaining solvent was removed by briefly applying vacuum at 120 °C. The plastic (and also clear, homogeneous) early post-gel mixture was pressed into a mold (30 × 10 × 1 mm) and cured at 120 °C for 3 days. No air was entering the mold during the process. Only stoichiometric formulations were prepared, the stoichiometry being defined by the molar ratio of functional groups r = (amino-H)/(epoxy) = 1. The formulations were calculated by replacing a part of the matrix amino component (D2000) by the amino-functional stannoxane nanofiller, so that the stannoxane amino protons exactly replaced the missing ones from D2000.

2.2.2. Nanofiller oligomerization via additional post-cure under argon

Post-cure (after normal cure) of the prepared nanocomposites was achieved by heating the samples to 180 °C under argon atmosphere for 12 h.

Oxidation treatment of the prepared nanocomposites was performed (after normal cure) by heating the samples to 180 °C in air for 12 h, using a forced circulation oven. The sample size was always identical: 30 mm height, 10 mm width, and 1 mm thickness. A small hole was drilled in the top of each sample, and the samples were hanging on a thin wire in the central part of the circulation oven, in order to ensure an optimal access of the circulating air.

2.2.3. Samples nomenclature

The Stannoxane ("Sn2") content in the formulations was quantified by the molar ratio of stannoxane amino-protons to all amino protons. For example the abbreviation "25-Sn2" describes a polymer, in which 25 mol% of amino-H-protons of D2000 (amino-H-tetrafunctional) were replaced by the appropriate amount of "Sn2" (amino-H-bifunctional). The curing conditions are also part of the sample names, e.g. "25-Sn2-n" means a normally cured sample, "25-Sn2-pcAr" endured an additional above-described post-cure under argon (nanofiller oligomerization), while "25-Sn2-ox" endured the above-described oxidation treatment (after the normal cure). Samples with the following mol % of amino groups from the stannoxane Sn2 nanofiller were prepared: 0.025, 0.05, 0.1, 0.5, 1, 4, 10, 17, 25, 50, 75 and 100% (names: "0.025-Sn2" – "100-Sn2"). The most important samples prepared are listed in Table 1, as well as their key parameters, and the determined gel fractions of matrix and nanofiller.

Table 1
Most important prepared samples and their gel fractions.

Sample name	mol % of Sn cage	wt % of Sn cage	Type of Sn cage	Additional post-curing	Fraction of gel w_g [ ]	w_g of filler [ ]	w_g of matrix [ ]
Matrix	0	0	None	NO	0.96	no	0.96
Matrix-pcAr	0	0	None	180 °C/12 h, under Ar	0.85	no	0.85
Matrix-ox	0	0	None	180 °C/12 h, in air	0	no	0
4-Sn2-n	4	8	Sn2	NO	0.97	0.97	0.97
4-Sn2-pcAr	4	8	Sn2	180 °C/12 h, under Ar	0.93	0.99	0.92
4-Sn2-ox	4	8	Sn2	180 °C/12 h, in air	0.88	1.0	0.87
10-Sn2-n	10	19	Sn2	NO	0.95	0.95	0.95
10-Sn2-pcAr	10	19	Sn2	180 °C/12 h, under Ar	0.92	0.98	0.91
10-Sn2-ox	10	19	Sn2	180 °C/12 h, in air	0.87	0.98	0.86
25-Sn2-n	25	40	Sn2	NO	0.81	0.83	0.80
25-Sn2-pcAr	25	40	Sn2	180 °C/12 h, under Ar	0.85	0.88	0.83
25-Sn2-ox	25	40	Sn2	180 °C/12 h, in air	0.78	0.82	0.75
50,75,100-Sn2-n	50–100	63–89	Sn2	NO	0[a]	0[a]	0[a]
50,75,100-Sn2-pcAr	50–100	63–89	Sn2	180 °C/12 h, under Ar	n.a.[b]	n.a.[b]	n.a.[b]
50,75,100-Sn2-ox	50–100	63–89	Sn2	180 °C/12 h, in air	n.a.[c]	n.a.[c]	n.a.[c]

[a] The samples are soluble in the extraction solvents' mixture.
[b] The samples do not dissolve, but have a problematic glue-like consistence.
[c] The samples do not dissolve, but are too fragile for sol–gel analysis.

2.3. Reactivity investigation

2.3.1. Preparation of samples for kinetics investigation

The samples for amino-functional stannoxane reactivity investigations were prepared in sealed ampoules at 120 °C. The starting concentrations of epoxy groups were 1 mol/L, those of amino groups 0.25 mol/L. Tested was the amino-functional stannoxane "Sn2" as well as a low-molecular-weight analogue of the amino-component in the prepared nanocomposites, poly(-oxypropylene) α,ω-diamine Jeffamine D230. As excess epoxy component, phenyl glycidyl ether (PGE) was used (which is chemically very similar to the nanocomposite component DGEBA). PGE, the tested amine (epoxy groups/amino protons ratio: 4/1), and 1-methyl-naphtalene standard (in 0.3/1 molar ratio to PGE) were mixed and diluted by toluene in order to achieve the above concentrations (1 M Ep and 0.25 M amino-H). The reaction mixture was divided into small ampoules and sealed. The ampoules were put into an oil bath at 120 °C. After the desired reaction time was reached, the respective samples were frozen instantly at −35 °C. Just before the analysis of the conversion degree via ^{1}H NMR the samples were dissolved in $CDCl_3$. (The investigated reactions proceed very slowly at room temperature and stand still in the timescale of weeks at the temperature of −35 °C).

2.3.2. Quantitative analysis via ^{1}H NMR

^{1}H NMR spectra used for the analysis of the conversion degree of epoxide-amine addition reactions were recorded on a Bruker (Karlsruhe, Germany) Avance DPX 300 spectrometer at 300 MHz. The concentration of the epoxy groups was determined by following the relative intensity (ratio (signal integral/standard signal integral)) of the oxirane-ring-H-signal near 3.32 ppm, which was always well-separated from all the other signals of starting compounds and of products. As internal standard the non-volatile 1-methyl-naphtalene was used, namely the integral of its well-separated aromatic signal at 7.80 ppm.

2.3.3. FT-IR investigation of stannoxane cage polymerization

Fourier-transform infrared spectroscopy investigations (FT-IR) were performed in an attenuated total reflection (ATR) mode using a Thermo Nicolet NEXUS 870 FTIR Spectrometer (Madison, WI, USA). Spectra of the powdered samples were measured with Golden GateTM Heated Diamond ATR Top-Plate (MKII single reflection ATR system; Specac; Orpington, UK).

2.4. Characterization of the nanocomposites

2.4.1. TEM

Transmission electron microscopy (TEM) was performed using the Tecnai G2 Spirit Twin 12 microscope (FEI, Czech Republic) after the thin samples (approximately 60 nm thick) were prepared by an ultramicrotome (Ultracut UCT, Leica, Germany) under cryogenic conditions (the sample and knife temperatures were −80 and −50 °C, respectively). The ultrathin sections were transferred to a microscopic grid and observed in the bright field mode at the acceleration voltage of 120 kV.

2.4.2. SAXS

SAXS experiments were performed using a pinhole camera (Molecular Metrology SAXS System) attached to a microfocused X-ray beam generator (Osmic MicroMax 002) operating at 45 kV and 0.66 mA (30 W). The camera was equipped with a multiwire gas-filled area detector with an active area diameter of 20 cm (Gabriel design). Two experimental setups were used to cover the q range of 0.005–4 Å^{-1}. The scattering vector, q, is defined as: $q = (4\pi/\lambda)\sin\theta$, where λ is the wavelength and 2θ is the scattering angle. The scattering intensities were put on an absolute scale using a glassy carbon standard. Calibration of primary beam position and sample-to-detector distances was performed using a silver behenate sample.

2.4.3. Fraction of gel and nanofiller extraction

2.4.3.1. Gel fraction of the entire nanocomposite. The sol–gel analysis of the nanocomposites prepared was carried out as follows: The samples were swollen and extracted with toluene/tetrahydrofuran (1:1). All the samples were extracted for 3 days while the solvent was changed every day for a pure charge. After the extraction, the samples were dried (vacuum, 100 °C) till weight constancy and the fraction of gel (w_g) was determined as:

$$w_g = \mathrm{mass(dry, after\ extraction)/mass(dry, before\ extraction)}.$$

The nanofiller extraction (via SnO_2 ash analysis) was determined as follows: The tested sample was divided into two pieces. Only one of these pieces was subjected to the above extraction. Both samples were subsequently subjected to ash analysis. Dividing the ash content of the extracted sample piece by the ash content of the non-extracted one directly yields the gel fraction of the nanofiller. The ash content for this calculation was expressed in %, relatively to the original sample weight. The ash analyses were performed as follows: The nanocomposite samples were first weighed and thereafter put into a platinum pot together with the double of their weight of sulfuric acid. This mixture was slowly pyrolyzed in air (heating at around 337 °C, the boiling point of H_2SO_4). The remaining ash was heated to ca. 1000 °C for 15 min. The pyrolysis with the sulfuric acid was repeated once more with the ash. The dry SnO_2 ash was then weighed.

The fraction of gel for the matrix alone was calculated from the gel fraction of the entire composite, from the gel fraction of the nanofiller and from the original (at synthesis) nanofiller content as follows:

$$w(m) = (1/(1-R))*w(g) - (R/(1-R))*w(f)$$

where:

$w(m)$ = gel fraction of the matrix alone
$w(g)$ = overall gel fraction of the entire composite
$w(f)$ = gel fraction of filler
R = original filler amount (= m(filler)/m(all))

2.4.4. DMTA

Dynamic mechanical properties of the nanocomposite products were tested with rectangular platelet samples, using an ARES G2 apparatus from TA Instruments. An oscillatory shear deformation (0.1%) at the constant frequency of 1 Hz and at the heating rate of 3 °C/min was applied, and the temperature dependences of the storage shear modulus and of the loss factor (G' and tan(delta), respectively) were recorded. The temperature range was typically from −100 to +120 °C (or −100 to +100 °C in case of nanocomposites which were not post-cured; in some cases the DMTA was recorded up to +150 °C). The geometry of the deformed area of all the tested samples was the same: 30 mm height, 10 mm width, and 1 mm thickness.

3. Results and discussion

3.1. Chemistry of the epoxy-stannoxane nanocomposites

In the presented study, four aspects of stannoxane chemistry played an important role: 1) the synthesis of the nanofiller, the

butylstannoxane dodecamer cages, 2) the reactive incorporation of this amino-functionalized stannoxane as into an epoxy matrix, 3) the stannoxane cages "polymerization" to larger domains, which can have strong effects on the nanocomposites' thermo-mechanical properties and on their morphology, and 4) the oxidative cross-linking reactions between the nanofiller and the matrix and among the nanofiller cages, which are responsible for the anti-oxidative action of the stannoxane nanofiller in the organic matrix.

3.1.1. Synthesis of the heavier POSS analogue, butylstannoxane dodecamer

The organo-tin-oxo cages generally can be synthesized similarly like their lighter POSS homologues (organo-silicon-oxo-cages) via the sol–gel process of the compounds $R{-}E(OH)_3$, where E is Si or Sn and R is an organyl group. While $R{-}Si(OH)_3$ is always highly reactive, the compounds $R{-}Sn(OH)_3$ are typically stable in the partly condensed form $[R{-}Sn(O)OH]_n$ and their further condensation must be enforced. A notable difference between POSS and stannoxane cages is the higher chemical reactivity of the latter, which is given by the metallic character of Sn: The stannoxanes can be dissolved not only by alkali (like POSS) but also by acids, and the Sn–C bond is also more easily broken than Si–C. The latter fact is important in tin-based anti-oxidants.

Dodecameric stannoxane cages, which were studied in this work, are most easily obtained with n-butyl substituents [28], by acid catalysed further condensation of $[R{-}Sn(O)OH]_n$ as shown in Scheme 3. Worth of notice are the sulfonate substituents, which are attached in axial positions of the stannoxane ellipsoid, which can be used to introduce functional groups.

In this work, the authors prepared a highly reactive, aliphatic-amino-functional stannoxane cage, "Sn2", with N-substituted amino groups, in order to achieve the nanofiller's rapid incorporation as linear units in the epoxy matrix. This was expected to enhance the nanofiller's anti-oxidative effect in the matrix, by making it more accessible in the more mobile linear segments of the matrix. The functional substituent, N-cyclohexyl-3-aminopropyl sulfonate, was chosen because of the commercial availability of the corresponding sulfonic acid and because of the easy separation and purification of the resulting stannoxane cage.

The three-step route of Ribot et al. [28,36] was used in this work to prepare "Sn2" (Scheme 3), starting from butyltin oxide hydroxide polymer, via the stannoxane dodecamer with toluenesulfonyl axial ionic substituents. The latter substituents were exchanged for hydroxy anions in the next step, which in turn were neutralized by cyclohexyl-3-aminopropanesulfonic acid, thus yielding "Sn2".

3.1.2. Nanocomposite formation

The elastomeric epoxy matrix based on poly(oxypropylene)-α,ω-diamine ("D2000", MW = 1968 g/mol, elastic component) and diglycidylether of bisphenol A (DGEBA) was chosen for the presented study because of its expected high sensitivity to reinforcing and to chemical effects of nanofillers. The neat matrix was prepared according to Scheme 4 and cured at 120 °C for 3 days. The matrix consists of rather rigid chains made from aromatic DGEBA units and N-atoms from D2000, which are interconnected with elastic polypropylene oxide chains. The latter connect N-atoms of the "rigid" chains.

The structure of the prepared nanocomposites with chemically bonded "Sn2" filler is derived from the structure of the neat matrix (see Scheme 5) by replacing a part of its amino-component, the elastic D2000 (amino-H-tetrafunctional; structure: two junctions connected by a spring) by "Sn2" nano-building blocks (amino-H-bifunctional, linear units). This results in a decrease of chemical crosslink density, although under favourable conditions some Sn2 units might form physical crosslinks via Sn2–Sn2 interactions.

The nanocomposite synthesis was performed similarly like the matrix synthesis. The nanofiller Sn2 was added as a 50 wt% solution in toluene. After gelation at 120 °C, the solvent was removed under vacuum, and the product was put into a mold and cured at 120 °C for 3 days. The use of solvent was necessary in order to assure a fine nanofiller dispersion.

The survival of the Sn2 cages under the conditions of the epoxy nanocomposite cure was evaluated on a liquid model system, in analogy to the method used by the authors in previous work [40]: The bifunctional epoxy matrix component, DGEBA (see Scheme 4) was replaced by its monofunctional analogue, phenyl-glycidyl ether. Liquid quantitative ^{119}Sn-NMR measurements, which compared the initial components' mixture and the mixture after standard cure, showed that the vast majority of the Sn2 cages, 75%, survived the cure intact.

3.1.3. Reactivity of the nanofiller's amino functions

In order to assess the process of stannoxane cages incorporation into the epoxy resin, the reactivity of Sn2 was investigated (see

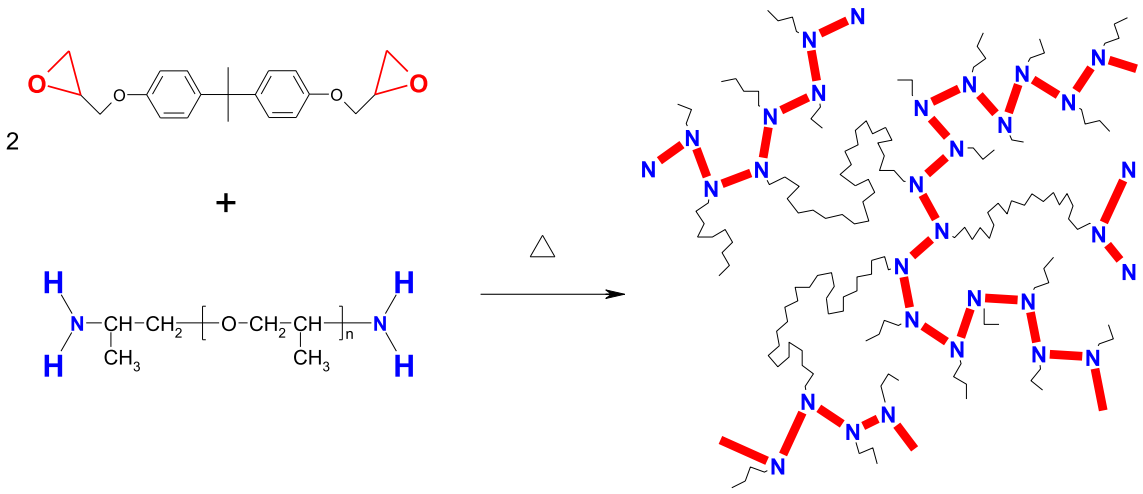

Scheme 4. Synthesis of the polymer matrix from diglycidylether of bisphenol A (DGEBA) and poly(oxypropylene) α,ω-diamine "Jeffamine D2000" (34-mer). In the matrix structure, DGEBA forms the more rigid chains (red, bold lines) which are interconnected by long elastic chains of D2000 (black thin lines) at the end of each DGEBA repeat unit. (For interpretation of the references to colour in this figure legend, the reader is referred to the web version of this article.)

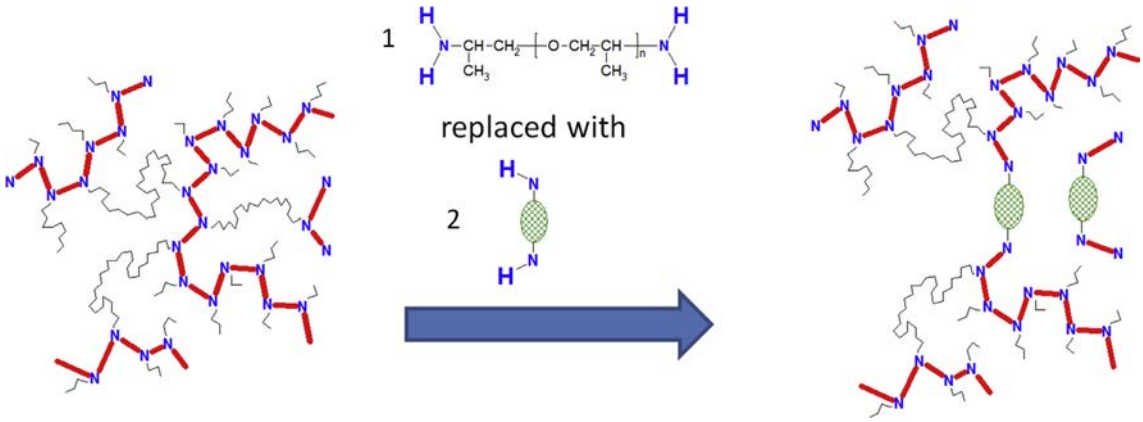

Scheme 5. Structure of the nanocomposite via replacement of a part of the branching and elastic amino-component of the matrix by the linearly bonded amino-functional stannoxane nanofiller Sn2.

Fig. 1): The stannoxane "Sn2" and poly(oxypropylene)-α,ω-diamine were reacted with a model epoxide, phenyl-glycidyl ether (chemically very similar to DGEBA) and their rate of conversion was compared. For convenience a short polypropylene oxide diamine was used, D230 (MW = 230 g/mol) in place of D2000 (1968 g/mol). The reaction was followed by means of ^{1}H NMR spectroscopy, by observing the decreasing intensity of the epoxy group signal at 3.30 ppm. It was preliminarily assumed, that the epoxy groups disappear only via addition reactions with amino groups.

In view of the results of the reactivity investigation (Fig. 1) it can be noted, that the amino-functional stannoxane reacts much faster with the phenyl-glycidyl ether than does the polypropylene oxide diamine D230 (the difference could be even greater with D2000 due to viscosity and buried-coil-end-effect). This result means a preferential reaction of Sn2 with the epoxy component DGEBA (Scheme 6), which is later followed by the reaction of the remaining DGEBA and of the epoxy-functional adducts "Sn2(DGEBA)2" with the less reactive amine D2000. This effect is expected to favour the fine dispersion of the nanofiller Sn2 in the epoxy matrix.

It also can be noted, that the stannoxane Sn2 significantly catalyses the epoxy groups homo-polymerization, which causes a further epoxy groups concentration decrease, even after all amino groups had reacted with epoxy. In the given experiments, the theoretical final epoxy group concentration should have been 75% of the starting value, as the ratio epoxy group:amino-H was 4:1. The rate of epoxide conversion slows down markedly in the region, where all amino protons should have reacted, so that the homo-polymerization can be considered to be slower than the epoxide-amine addition. This side reaction could contribute to somewhat higher fractions of sol (as non-bonded D2000 diamine) in nanocomposites with high Sn2 content. As can be seen further below, a marked effect of this side reaction was not observed.

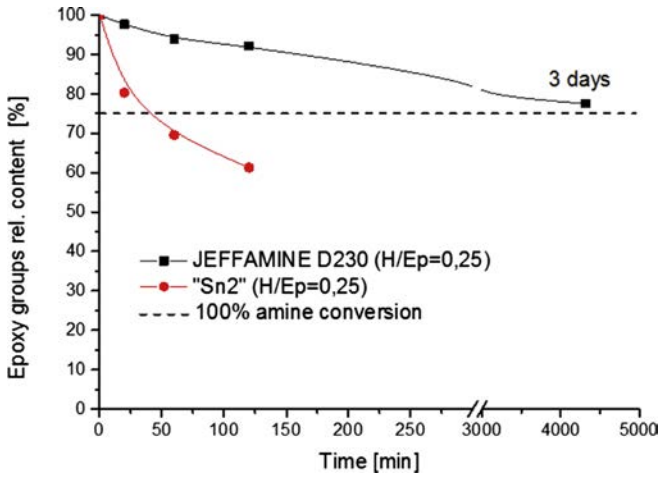

Fig. 1. Relative reactivity: kinetic curves of consumption of epoxy functions of phenyl glycidyl ether (which is chemically very similar to the epoxy component of the matrix, DGEBA), in reaction with the amino-functionalized nanofiller "Sn2" and with Jeffamine D230, a low-molecular-weight analogue of the amino component of the matrix. T = 120 °C, in sealed ampoule, r(H(−N)/Ep) = 0.25, c_0(Ep) = 1 M, c_0(Am) = 0.25 M, in toluene, epoxy groups are assumed to disappear by reaction with amine.

3.1.4. Polymerization of stannoxane nano-building blocks to larger domains

The lability of the butylstannoxane dodecamer cages at high temperatures was reported in earlier work [28,40]. The neighboring stannoxane cages rearrange to larger irregular structures, the ^{119}Sn-NMR peaks of which are very broad and usually invisible [40]. A likely mechanism of this cage polymerization, as suggested by the authors, involves the functional-group-carrying substituents, which are attached in axial positions to the ellipsoid cages via oxonium ionic bonds. According to the suggested mechanism, the oxonium bonds would dissociate (see Scheme 7) similarly like ammonium salts upon sublimation.

After the oxonium bond dissociation cage rearrangement and re-protonations by the sulfonic acid are expected to occur. Finally, the "damaged" and reactive cages collide and merge to larger structures. It is worth of notice that, the acidic protons play a key role as reactant and catalyst in the stannoxane cage formation from the polymeric butyltin oxide hydroxide (Scheme 3): An excess of 3.5 sulfonic acid groups per 12 Sn atoms is used for optimal yields, instead of the stoichiometric ratio of 2 SO_3 per 12 Sn [28].

The progress of stannoxane cage polymerization can be observed – in case of soluble model systems – via ^{119}Sn-NMR [40], as decrease of intensity of the two Sn peaks typical for the cluster, at −273 ppm (5-coordinated equatorial Sn atoms on the ellipsoid cage) and −453 ppm (6-coordinated Sn atoms on polar circles of the cage). On the other hand, the changes in ^{1}H NMR spectra are less sweeping: little difference is observed after Sn2 polymerization (the NMR spectra are not depicted).

3.1.4.1. FT-IR investigation of the Sn2 polymerization. The changes in the molecular structure of the neat cage Sn2 during gradual heating have been studied using ATR FTIR spectroscopy on a diamond crystal (see Fig. 2). After heating to 60 and 100 °C we observe only

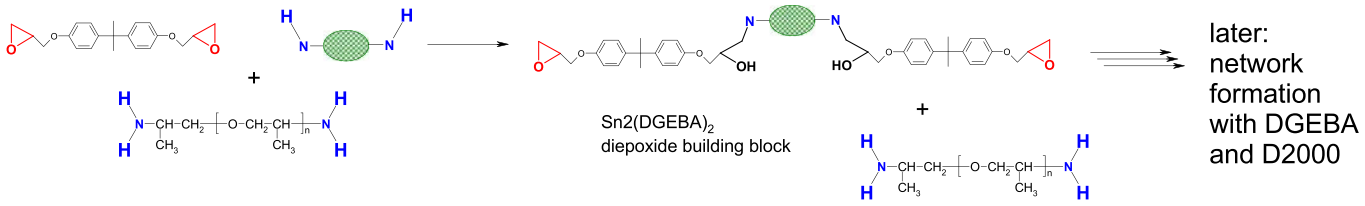

Scheme 6. The preferred reaction of the nanofiller with the epoxy component.

small changes in the intensity ratio of the doublet at 1199/1179 cm^{-1} and a small shift of the peak at 1035 cm^{-1}, both belonging to SO_3 stretching vibrations of the functional-group-carrying substituents of Sn2 (Fig. 2A). After heating to 120 °C the second maximum at 1199 cm^{-1} in the above mentioned doublet disappears and the peak at 1035 cm^{-1} shifts to lower wavenumbers. In the high wavenumbers region we observe a new maximum at 3234 cm^{-1} positioned on a broad peak of O—H and N—H stretching vibrations. The new, relatively sharp maximum can be assigned to the stretching vibrations of newly appearing hydrogen bridged O—H groups (Fig. 2B).

Some changes in the region of stretching vibrations of C—H groups at 2870/2855 cm^{-1} and of corresponding bending vibrations at 1462/1453 cm^{-1} and rocking vibrations at 722/707 cm^{-1} are also observed. These changes can be correlated with small changes or distortions in the Sn2 cage structure. The IR spectrum remains unchanged (after 30 min) once the sample reached 120 °C. The spectrum of a rapidly polymerized (at 240 °C) Sn2 sample is shown for comparison in Fig. 2. According to previous investigations [40], the polymerization is immediate at this temperature. The spectrum displays similar changes like those observed during gradual temperature increase. The small sharp peak of H-bridged OH disappears, and the peaks assigned to the SO_3 groups experience some additional small changes. The sharp OH peak is hence probably connected with temporary stannoxane cage species, which are protonated at different than the original axial O atoms. These temporary species likely play a key role in the Sn2 cage re-organization to larger structures.

The described observations support the above suggested mechanism of stannoxane cages polymerization via dissociation and repeated formation of oxonium bonds.

Finally, morphology investigations, which are discussed further below, strongly support the suggested mechanism of oxonium bonds dissociation: Nanofiller movement under formation of distinct and relatively large stannoxane nano-domains (which could contain hundreds of original cages) was observed as result of annealing at 180 °C, although the nanofiller was found to be practically inextractable at room temperature, and the morphology prior to annealing was highly homogeneous. The movement could be easily made possible by the thermal dissociation of the functional substituents, which would set free the nanofiller building blocks.

3.1.5. *Oxidative crosslinking reactions of the stannoxane cage*

It was found by the authors recently, that the stannoxane nano-building blocks undergo oxidative crosslinking reactions in epoxy matrices containing polypropylene oxide chains, and that these reactions counteract the oxidative degradation of the matrix [40]. This effect was especially visible on the thermo-mechanical properties. The reactions (Scheme 8) were shown to involve crosslinking between nanofiller and matrix and filler—filler crosslinking. The reactions were investigated on a model liquid system [40], which could be analysed via NMR and rheology. The filler-matrix crosslinking made itself apparent by the decrease of the signals of the n-butyl substituents of stannoxane in ^1H NMR [40] as well as by a marked increase in viscosity [40]: Gelation is observed in extreme cases, while the neat matrix degrades and its viscosity decreases under the same conditions. Chemical attachment of previously non-bonded stannoxane to the matrix was also observed [40], which led to characteristic changes of mechanical properties. The stannoxane—stannoxane crosslinking can make itself apparent as

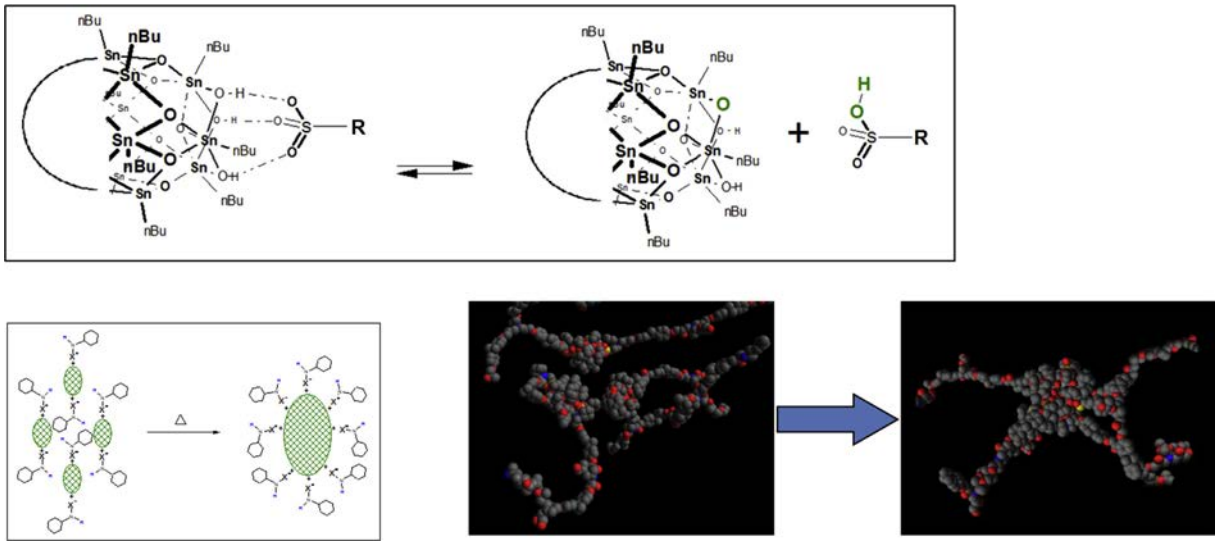

Scheme 7. Stannoxane polymerization and its probable starting step, oxonium salt dissociation.

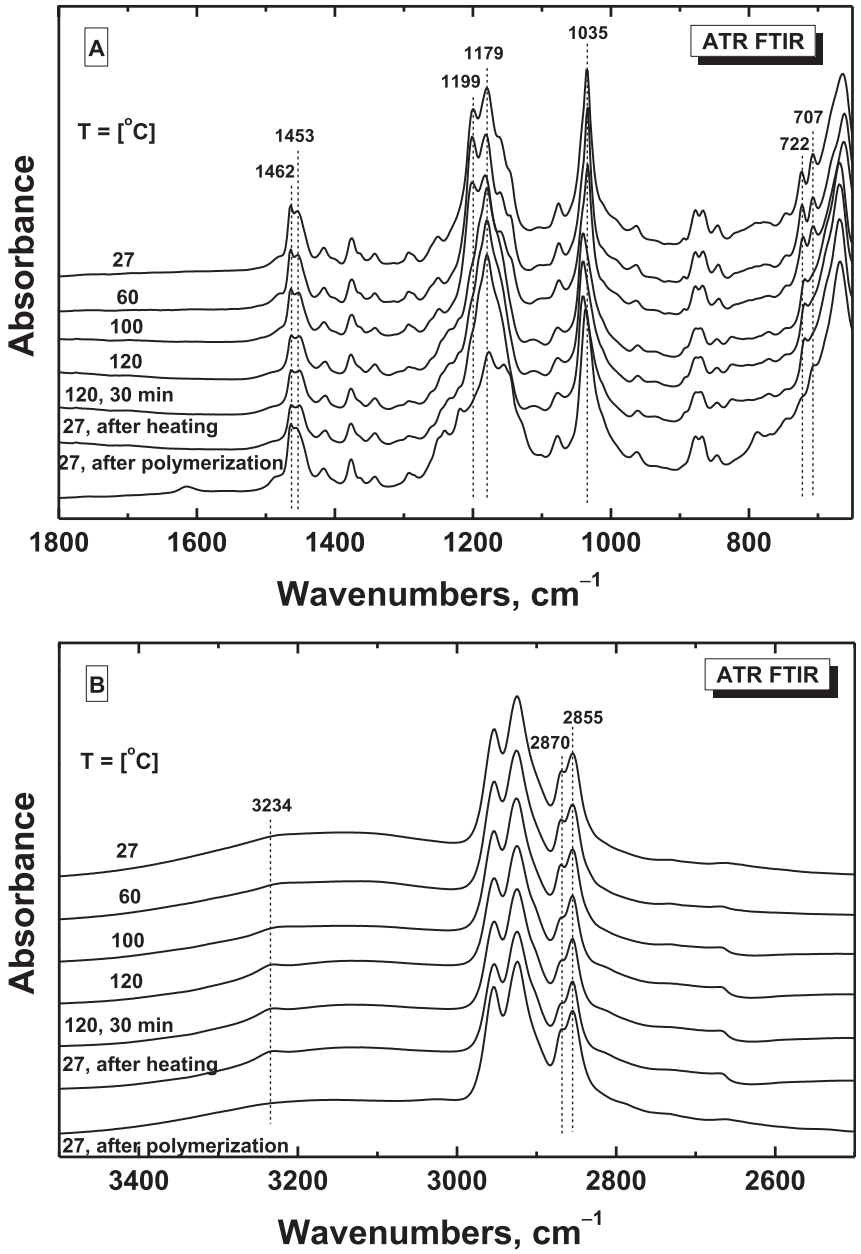

Fig. 2. ATR FTIR spectra of a neat Sn2 cage sample heated to 27, 60, 100, 120 (repeated measurement after 30 min), and thereafter cooled back to 27 °C. A spectrum of a sample rapidly polymerized at 240 °C is shown for comparison. Top: range of sulfonate groups stretching vibrations and of aliphatic C—H bending and twisting; Bottom: range of O—H and N—H stretching.

SnO_2 precipitation in the case of intense oxidation of the liquid model system.

In this work, finely dispersed stannoxane nano-building blocks "Sn2", incorporated as well-accessible and somewhat mobile linear segments in the epoxy matrix, were expected to achieve a markedly higher anti-oxidative activity than the previously studied "Sn4" nanofiller [40], which was a branching building block and which displayed aggregation to nano-domains, thus being less accessible for oxidative crosslinking reactions.

3.2. Nanofiller dispersion in the epoxy matrix

Nanofiller dispersion and its bonding to the matrix was studied by Transmission electron microscopy (TEM), small-angle X-ray scattering (SAXS), and by extraction and ash analysis. Nanocomposites after standard cure, after additional annealing for 12 h at 180 °C under argon, or after oxidation treatment (of standard-sized specimens) via 12 h heating at 180 °C in circulating air were investigated and compared.

3.2.1. Morphology of the obtained nanocomposites

3.2.1.1. TEM. The TEM investigations show interesting results: The Sn2 nanocomposites with the epoxy matrix are highly homogeneous after the standard cure at 120 °C (Figs. 3 and 4a1—e1). Eventual heterogeneities are smaller than 10 nm. At the highest nanofiller concentrations, some occasional heterogeneities can be observed.

After annealing for 12 h at 180 °C under argon (Figs. 3 and 4a2—e2), the morphology is distinctly different: At lower Sn2 concentrations, occasional nano-domains newly appear. At 10 mol%

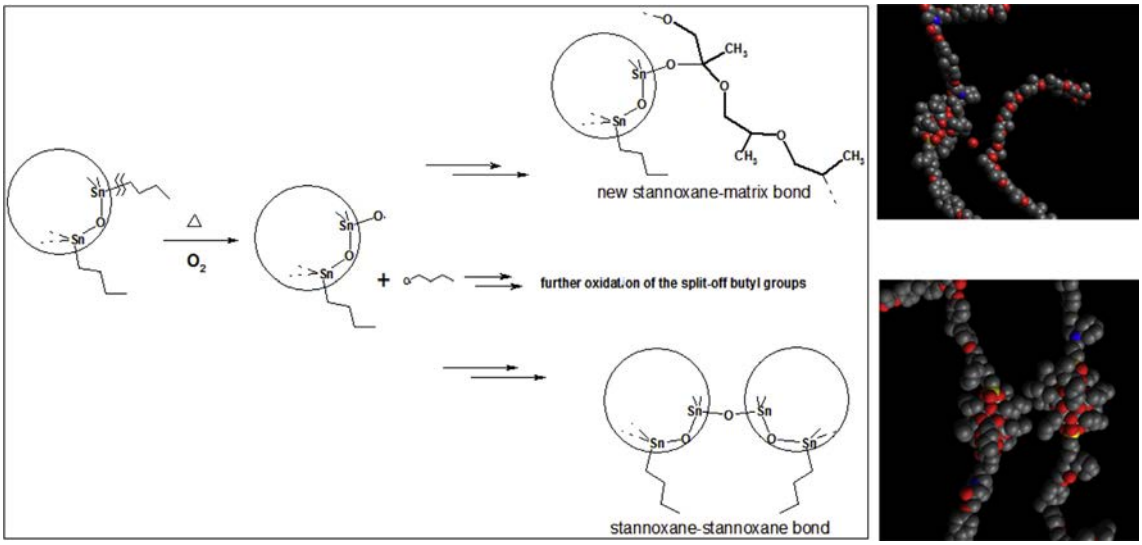

Scheme 8. Oxidative crosslinking reactions of the stannoxane nano-building blocks with the matrix and with each other, as proven by ^{1}H NMR experiments in Ref. [40].

(19 wt%) Sn2, numerous elongated nano-domains are formed, sized around 15 × 80 nm (or 7 × 15 stannoxane units), which in case of densest packing would contain hundreds of Sn2 cages. At even higher nanofiller contents, extended stannoxane-rich regions alternate with matrix-rich ones. At 50 mol% (63 wt%) the stannoxane-rich phase is continuous after the annealing, while the matrix-rich phase forms spherical inclusions. In view of the high reactivity of the nanofiller towards epoxies (see above) and of its

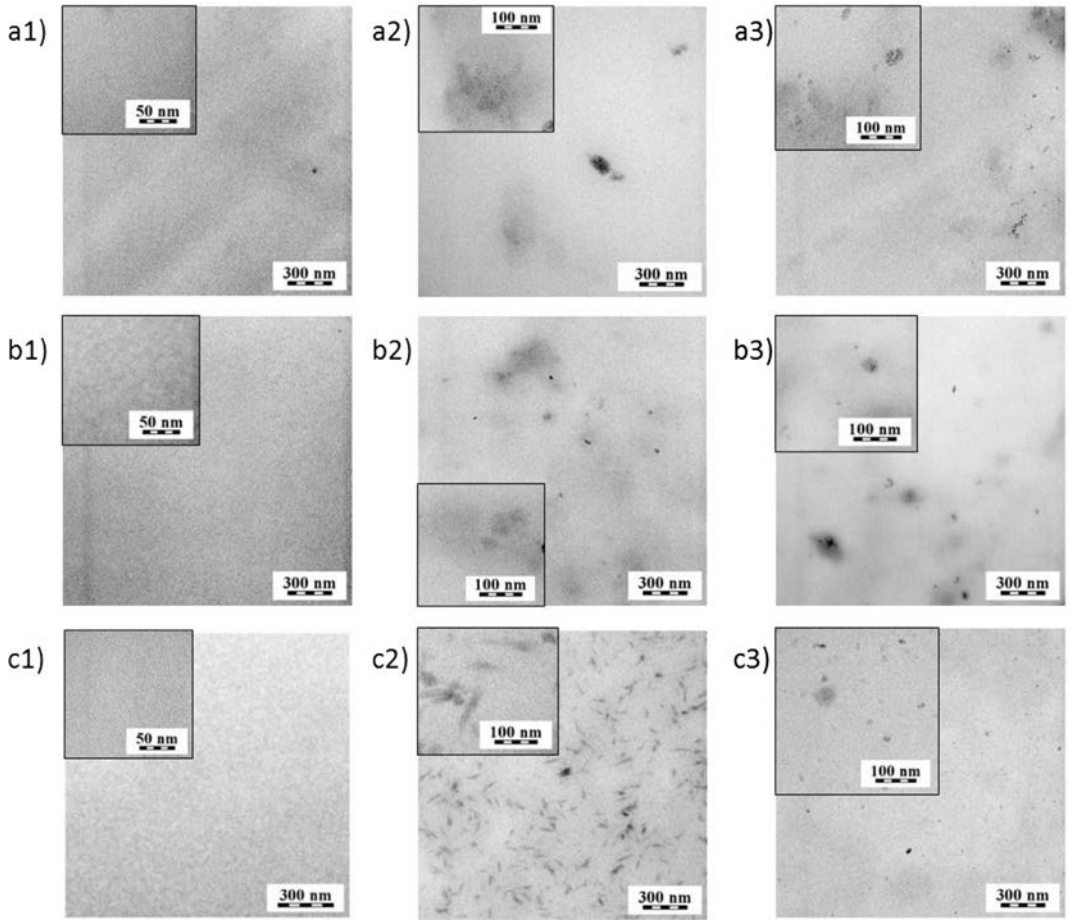

Fig. 3. Transmission electron microscopy images of Sn2 nanocomposites with DGEBA-D2000: with 1 mol% Sn2 (a1−a3), 4 mol% Sn2 (b1−b3), and 10 mol% Sn2 (c1−c3), which underwent normal cure (a1, b1, c1), additional 12 h post-cure under argon (a2, b2, c2), or additional 12 h oxidation treatment (a3, b3, c3).

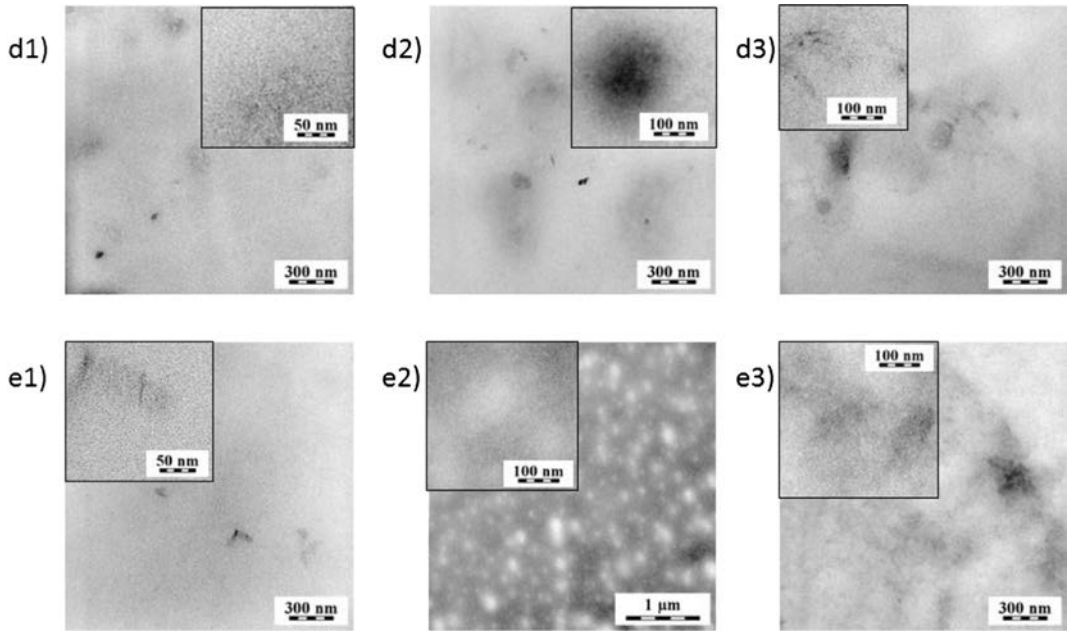

Fig. 4. Transmission electron microscopy images of Sn2 nanocomposites with DGEBA-D2000: with 25 mol% Sn2 (d1—d3), and 50 mol% Sn2 (e1—e3), which underwent normal cure (d1, e1), additional 12 h post-cure under argon (d2, e2), or additional 12 h oxidation treatment (d2, e2).

practical inextractability (see Table 1 below), the observed "nano-precipitation" can only be explained by a short-range nanofiller mobility during the annealing process, as discussed above in the section about the nanocomposites' chemistry.

The above suggested mechanism of high-temperature dissociation of the functional group-carrying substituents bonded via oxonium ionic bonds to the Sn2 cages makes possible their detachment from bonded positions in the matrix, and the subsequent movement of the small nano-building blocks until they collide with each other and polymerize to larger structures (see Scheme 9).

The situation is different under the oxidation treatment conditions (see Figs. 3 and 4a3—e3): The stannoxane building blocks movement and their subsequent merger to extended domains is markedly hindered by the oxidative crosslinking reactions, which attach the stannoxane cages to the matrix by strong covalent bonds. Hence, only smaller and occasional nano-domains form, and the morphology is more homogeneous after the oxidation treatment, in contrast to samples annealed under argon.

3.2.1.2. SAXS. The phase structure of the nanocomposites after standard cure, after annealing under argon and after oxidation treatment was analysed by means of small-angle X-ray scattering (SAXS). The results are illustrated in Figs. 5—8.

The neat nanofiller, Sn2, displays interference signals (Fig. 6) which form two multiplets of peaks. The multiplet at scattering vector (q) values between 2.79 and 1.13 A^{-1} corresponds to characteristic distances between 0.22 and 0.56 nm, and was assigned to intramolecular distances in the butyl and cyclohexyl substituents of the Sn2 organo-tin-oxo cage. These signals are found in the region of the broad amorphous halo of the organic polymer matrix, which correspond to intermolecular distances of hydrocarbon chains around 0.44 nm (see Fig. 6). The matrix also displays a broad flat maximum around 0.15 A^{-1} which corresponds to the distance of 4.2 nm and which can be assigned to coiled polypropylene oxide chains of D2000.

The second and highly characteristic multiplet of Sn2 interference signals is observed between q values of 0.83 and 0.44 A^{-1}, corresponding to 0.76—1.42 nm, which was assigned to the dimensions of the heavy inorganic core of Sn2 (intramolecular distance). The characteristic signal of the inorganic core of Sn2 is observed in all the prepared composites, as a step or as a broad peak at higher filler concentrations, although at 1 mol% (2 wt%, sample "01-Sn2") it is already very weak. The signal is also observed after

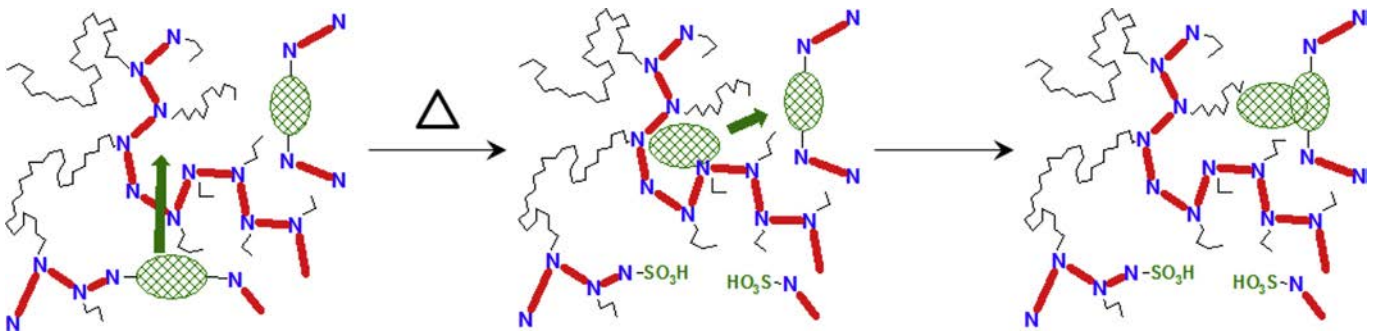

Scheme 9. Schematic representation of the Sn2 nano-building blocks polymerization to larger domains, which is enabled by short-range Sn2 mobility.

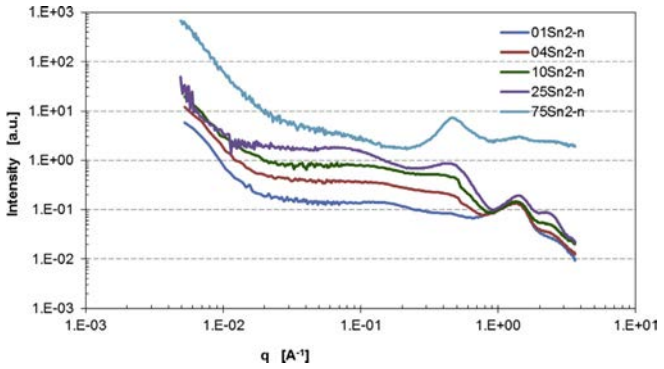

Fig. 5. SAXS scattering patterns of epoxy nanocomposites with different contents of Sn2, ranging from 1 mol% to 75 mol%, corresponding to 2–76 wt%, after normal cure at 120 °C.

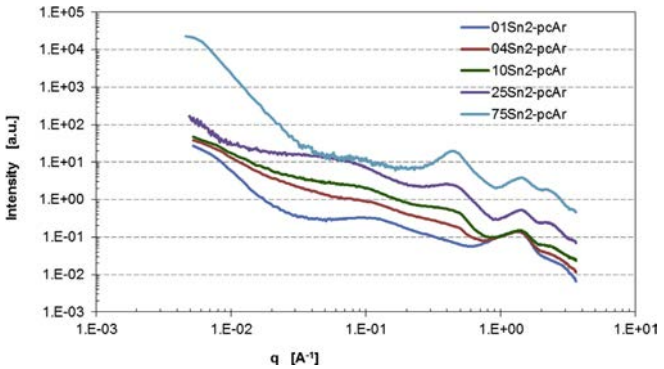

Fig. 7. SAXS scattering patterns of epoxy nanocomposites with different contents of Sn2, ranging from 1 mol% to 75 mol%, corresponding to 2–76 wt%, which were additionally post-cured under argon (12 h at 180 °C).

annealing or oxidation: it displays a maximum at $q = 0.49$ A^{-1} in the normally cured composites, corresponding to 1.3 nm, while in the samples which were post-cured under argon or oxidized, the maximum is slightly shifted to $q = 0.45$ A^{-1} (1.4 nm distance). This finding indicates, that a significant fraction of the cages remains preserved, at least in their overall size, also in the annealed and oxidized samples.

At lower values of the scattering vector, around 0.1 A^{-1}, a step is observed in the normally cured nanocomposites and in those annealed under argon. In the oxidized samples, there is rather a broad peak in the same place. This feature might be assigned to nanofiller aggregation at higher concentrations to small domains composed of a few cages. The positions of the step edges or of the maxima lead to the characteristic sizes of 4–10 nm in concentrated normally cured nanocomposites, 5–11 nm in the ones annealed under argon and 7–8 nm in the oxidized ones. In the case of the annealed samples, this characteristic distance can be correlated with the width of the stannoxane-rich domains observed via TEM. Similarly the characteristic distance for the oxidized samples can be connected with the diameter of the smaller, mostly spherical domains visible by TEM.

Interesting is also the scattering pattern in the region of $q = 0.015$–0.005 A^{-1}: The nanocomposites cured normally and those after oxidation treatment display a steep increase in the scattering intensity with decreasing scattering vector, which is consistent with a dispersion of particles with a high fractal dimension in the matrix, e.g. of nearly spherical single cages, or of small or larger spherical domains. The oxidized samples with a lower Sn2 content display a somewhat flatter slope, suggesting a lower fractal dimension of heterogeneities. Most of the samples annealed under argon display flatter slopes (except at the highest Sn2 content of 75 mol%) in the discussed region, which corresponds well with the lower fractal dimension of the elongated nanofiller-rich domains which were observed by TEM.

3.2.2. Nanofiller extractability

The efficiency of nanofiller bonding to the epoxy matrix was investigated by extraction experiments. The overall gel fraction was determined via extraction with a 1:1 toluene-tetrahydrofuran mixture, which dissolves well the components of the matrix as well as the neat nanofiller. Additionally, ash analysis (stannoxane conversion to SnO_2) was performed on the tested samples before and after extraction, in order to directly determine the nanofiller extractability. The results were compared with extraction tests on the neat matrix.

The results of extraction and ash analyses show (see Table 1), that the nanofiller is incorporated in the epoxy matrix with a high efficiency after the standard cure, which correlates with its high reactivity (discussed above) towards the epoxy component. The neat matrix displays a marked thermal degradation after 12 h annealing under argon at 180 °C (gel fraction decreases from 0.96 to 0.85), and it degrades to a soft soluble solid (gel fraction = 0) after the oxidation treatment (12 h in circulating air at 180 °C). With the stannoxane nanofiller, the decrease of the gel fraction after annealing under argon is more moderate, obviously because additional crosslinks are formed via stannoxane cages oligomerization to larger units. This effect can be seen also on the mechanical properties discussed below. The dramatic decrease of the gel

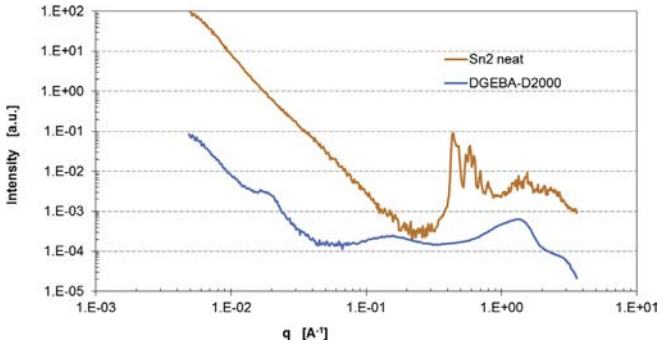

Fig. 6. SAXS scattering patterns of the neat nanofiller Sn2 and of the neat DGEBA-D2000 matrix, after normal cure at 120 °C.

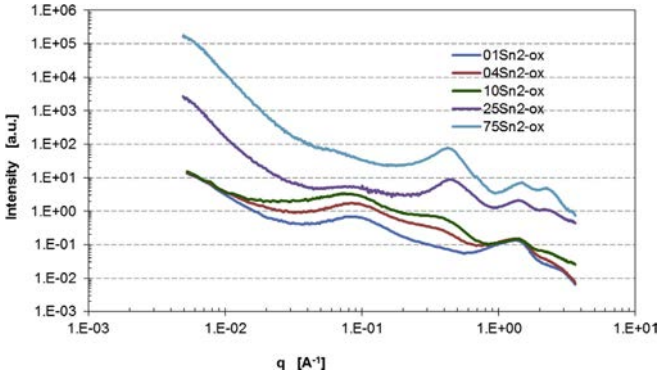

Fig. 8. SAXS scattering patterns of epoxy nanocomposites with different contents of Sn2, ranging from 1 mol% to 75 mol%, corresponding to 2–76 wt%, which additionally received oxidation treatment (12 h in circulating air at 180 °C).

fraction upon oxidation treatment is strongly counter-acted by the stannoxane nanofiller, the gel fractions of the oxidized nanocomposites are only somewhat smaller than in the case of analogous samples annealed under argon. The nanofiller incorporation (see w_g of filler, Table 1) in the nanocomposites remains high after annealing or oxidation, which can be explained by additional filler—filler- (after annealing) or filler-matrix-crosslinks (after oxidation). Analysis of the extracted sol by means of ^{1}H NMR shows, that the main extracted component are polypropylene oxide chains (signals at 1.12, 3.39 and 3.55 ppm), while some amount of DGEBA derivatives is also present (aromatic signals at 6.72 and 7.04 ppm), as well as some butyl groups (α-CH_3 at 0.92 ppm) which originally belonged to the stannoxane. Small amounts of tin can be proven in the extract by ash analysis, but changes in the nanofiller bonding to matrix are more precisely determined by ash analysis of extracted nanocomposite samples before and after oxidation. Further it can be observed, that with the increasing content of the linearly bonding nanofiller Sn2, which replaces the elastic and at the same time branching amino-component of the matrix, D2000, the gel fraction of the composites decreases, more markedly above 10 mol % (19 wt%) Sn2. This is obviously the consequence of a decreasing crosslink density in the nanocomposites.

3.3. Thermo-mechanical properties

The incorporated linearly bonded stannoxane nanofiller Sn2 has a marked influence on the thermo-mechanical properties of the prepared nanocomposites. The nanofiller effect also strongly depends on the nanocomposites history after their standard cure at 120 °C: Because of oxidative crosslinking reactions, the reinforcement by the Sn2 nanofiller is extremely strong after the oxidation treatment of the nanocomposites.

The normally cured epoxy-Sn2 nanocomposites display simple trends in their thermo-mechanical properties (see Fig. 9). The curves of the temperature dependence of the storage shear modulus (G') are similar in shape for the nanocomposites and for the neat DGEBA-D2000 epoxy matrix, but the glass transition region (step in G') shifts to higher temperatures, due to the immobilizing effect of the rigid and heavy Sn2 cages in the polymer network, and at higher concentrations, also due to Sn2—Sn2 interactions. The increase in the content of the linearly bonding Sn2 units, which replace the branching D2000 amino-component, also leads to a decrease of the modulus in the rubber plateau and eventually at the highest Sn2 contents to melting. At 100 mol% Sn2, the nanofiller shifts the glass transition by 70 °C.

The temperature dependence of the loss factor tan(δ) illustrates the thermal transitions in the nanocomposites. The peak of the unhindered relaxation of the polypropylene oxide (D2000) chains is observed near −29 °C (maximum) in the neat matrix. With increasing content of the Sn2 nanofiller, a shoulder on the mentioned peak appears on its higher-temperature slope, the whole peak eventually shifts to higher temperatures (from −29 to −8 °C) and becomes smaller, while on its lower-temperature-slope a shoulder corresponding to the relaxation of the decreasing fraction of unhindered D2000 chains can be observed. At very high Sn2 contents, 50 mol% and above, the D2000 peak disappears. At Sn2 concentrations above 4 mol% (8 wt%) a small (till 17 mol%) flat peak near +10 °C appears, which can be assigned to the relaxation of Sn2-rich segments in the nanocomposite. The latter are expected to consist mainly of Sn2 and DGEBA (high Sn2 reactivity towards DGEBA) and of some D2000. With increasing Sn2 content this transition becomes prominent, its maximum shifts to higher temperatures (decrease of the content of soft D2000 in the segments) and at 50 mol% (63 wt%) it becomes the only significant transition, with a broad peak centred around 60 °C. The extended Sn2-rich segments dominate the thermo-mechanical behavior at this concentration. At 75 and 100 mol% (DGEBA-Sn2 resin without D2000) the nanocomposites display a melting transition, because they are not sufficiently crosslinked. The 100-Sn2 nanocomposites display two small peaks at +25 and +45 °C, which could be assigned to relaxations of DGEBA segments (neat DGEBA melts at +48 °C). The melting point of the neat Sn2 nanofiller was determined to be near 113 °C, which is a somewhat higher temperature than in the case of the melting range of 100-Sn2.

3.3.1. After polymerization

The annealing at 180 °C under argon has a marked effect on the thermo-mechanical properties of nanocomposites with Sn2 contents of 10 mol% (19 wt%) and higher (see Fig. 10). If the curves $G' = f(T)$ are compared, the step in G' which corresponds to the glass transition region is shifted to higher temperatures. Secondly, the trend of decreasing storage moduli G' in the rubber plateau is nearly stopped at the higher Sn2 contents, obviously due to additional crosslinks formed by the merger of linearly bonding Sn2 nanobuilding blocks to larger polyfunctional nanoparticles. This effect outbalances the reduction in crosslink density by incorporating bifunctional Sn2 in place of tetra-functional D2000, and also the thermal degradation of the matrix, which can be also observed on the sample without nanofiller. Consequently, the 100-Sn2-pcAr composite does not melt (and also does not dissolve during extraction experiments, see above), in contrast to the normally cured 100-Sn2-n. The curves $G' = f(T)$ are less steep in the glass transition region than for samples which were normally cured, especially at higher Sn2 contents. This indicates a relatively broad range of structures formed by the polymerization of Sn2, which accordingly relax at different temperatures.

The curves $\tan(\delta) = f(T)$ of the annealed samples display similar trends like in the case of normally cured ones, but the relaxation peak of the stannoxane-rich phase is more prominent even at lower concentrations, and at 100 mol% Sn2, a relaxation peak is observed near 110 °C, in place of a melting transition near 70 °C. The relaxation of the stannoxane-rich phase is shifted to higher temperatures: From 30 to 110 °C instead of 10—70 °C in case of normal cure.

3.3.2. After oxidation

After the oxidation treatment (heating in circulating air at 180 °C for 12 h), the nanocomposites are strongly reinforced by oxidative crosslinking reactions between matrix and nanofiller (and at high Sn2 contents also by Sn2—Sn2 crosslinking). Sn2 polymerization is also likely to occur to some extent, but the crosslinking reactions with single Sn2 units seem to be faster, as the above discussed morphology results indicate. The neat matrix degrades to a soft solid after the oxidation treatment, and it dissolves upon attempted sol extraction (a complete degradation to liquid occurs in about 18 h). The DMTA curve of the degraded matrix is shown in Fig. 11. Already at extremely low contents of the Sn2 nanofiller, 0.025 mol% (0.05 wt%), a marked mechanical matrix stabilization via additional Sn2-matrix crosslinking can be observed. At 0.5 mol% (1 wt%) Sn2, the oxidized nanocomposite displays similar properties, like the neat matrix before oxidation. At 1 mol% (2 wt%), the nanocomposite is significantly reinforced (instead of degradation) after the oxidation treatment, but still comparable with the original matrix. At higher Sn2 contents, the nanocomposite reinforcement by oxidative crosslinking dramatically increases, above 10 mol% (19 wt%) Sn2, the oxidized nanocomposites are hard and brittle, and their glass transition is only moderate. The samples with 50 mol% and more Sn2 were too brittle for the DMTA analysis. The curves $\tan(\delta) = f(T)$ of the oxidized composites display broadened relaxation peaks of the

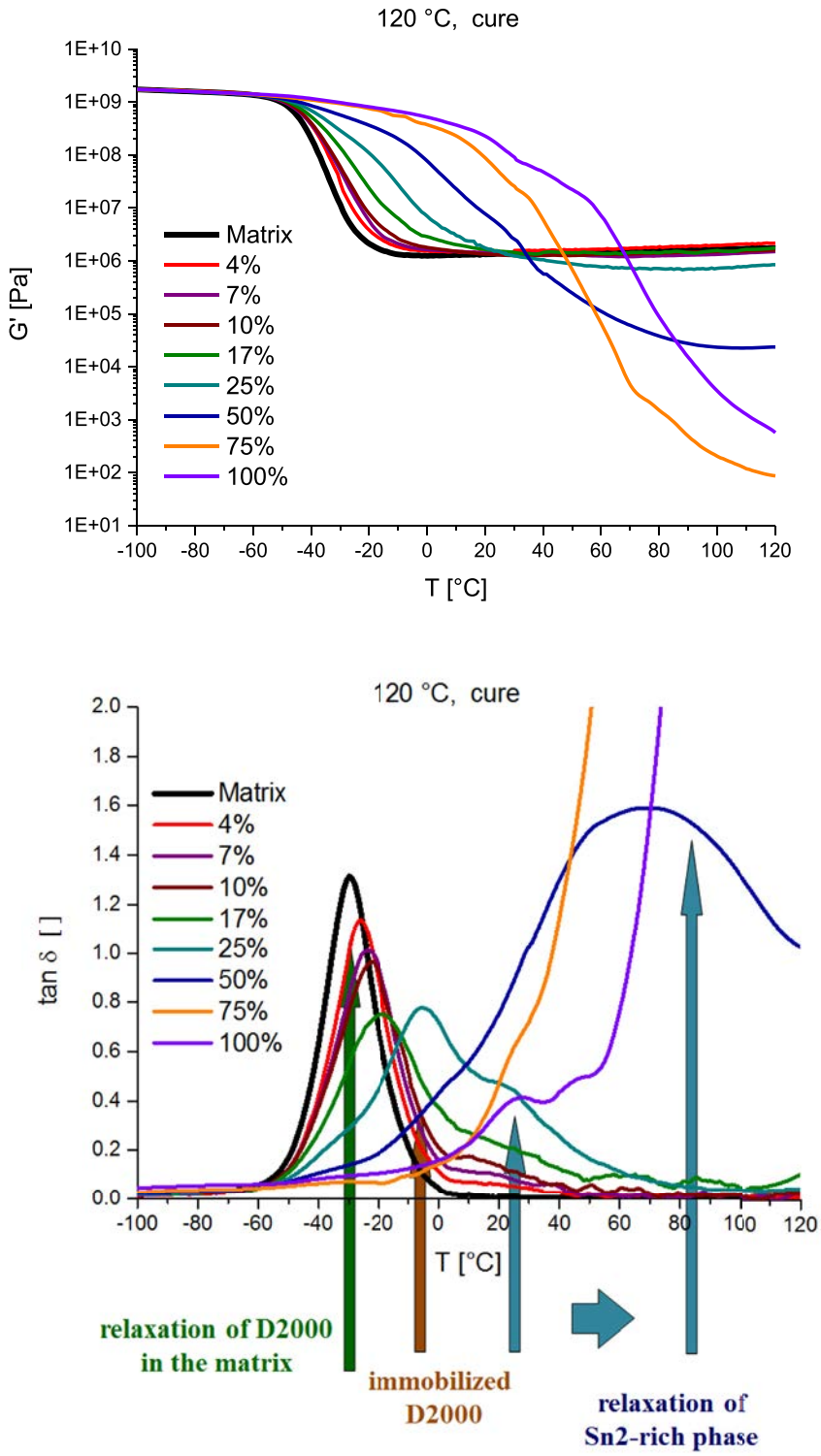

Fig. 9. Effect of nanofiller content on the thermo-mechanical properties of normally cured epoxy-Sn2 nanocomposites: Shear storage modulus *G'* (top) and loss factor tan(δ) (bottom, with assignment) as function of temperature: nanofiller content is in the range of 4–100 mol% amino protons.

D2000 chains as main feature. These peaks become increasingly flatter with increasing Sn2 content. This effect can be assigned to the increasing crosslinking and hence immobilization of the matrix with Sn2 units which also leads to a smaller step in the $G' = f(T)$ curve. The broadening of the glass transition peak in the neat matrix after oxidation can be connected with the oxidative damage to its regular structure, leading to friction of branched matrix segments on each other; the peak does not decrease in height, but increases more than twice in area. The relaxation peak of the stannoxane-rich phase appears distinctly only at 25 mol% Sn2 as a flat broad peak, whose maximum is at a much higher temperature (+90 °C) than in the case of analogue samples normally cured (+25 °C) or annealed under argon (+55 °C).

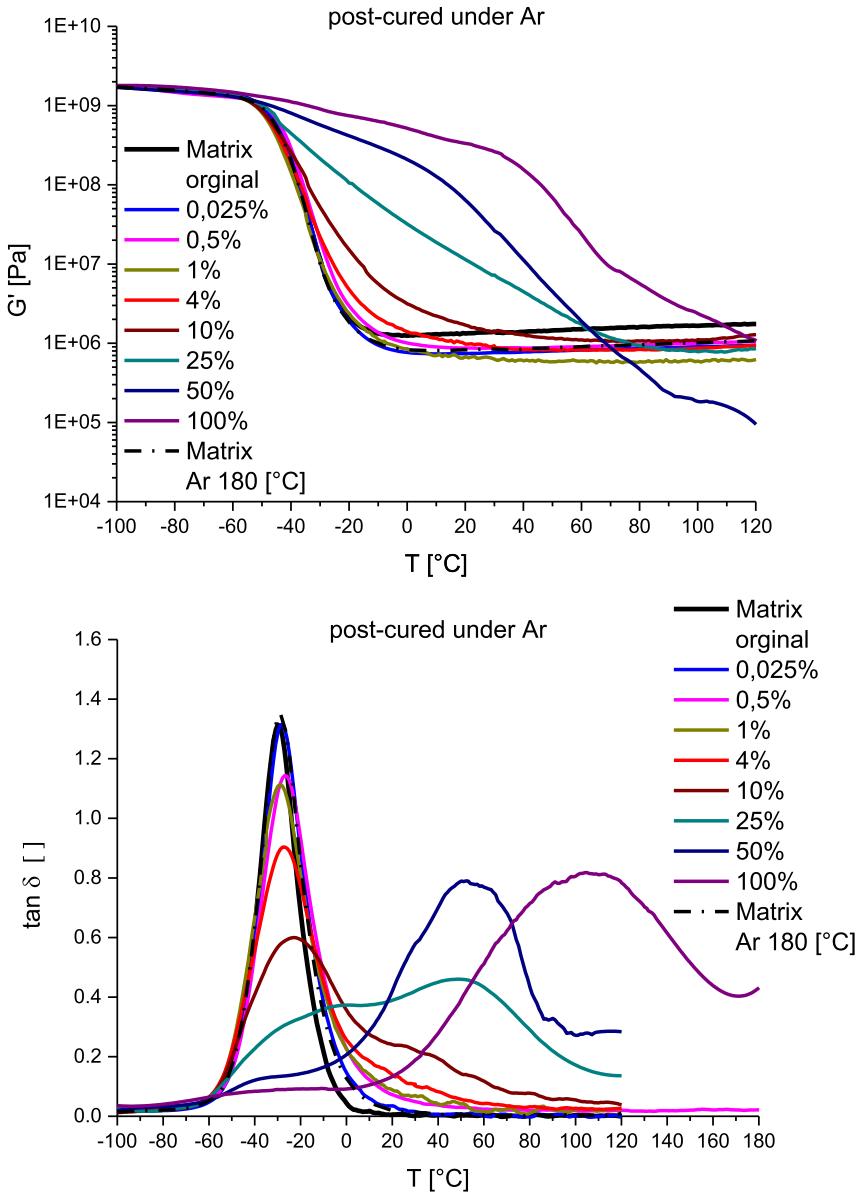

Fig. 10. Effect of nanofiller content on the thermo-mechanical properties of the epoxy-Sn2 nanocomposites which underwent post-cure under argon (nanofiller polymerization): Shear storage modulus *G'* (top) and loss factor tan(δ) (bottom) as function of temperature: nanofiller content is in the range of 0.025–100 mol% amino protons.

3.4. Comparison of POSS and its stannoxane analogue

If the homologues POSS (polyhedral oligomeric silsesquioxane) and butylstannoxane cages are compared in their effect on thermo-mechanical properties of nanocomposites, certain trends can be noted. In Fig. 12, the thermo-mechanical properties are compared of epoxy-Sn2 nanocomposites and of the previously synthesized [25,26] nanocomposites of the same DGEBA-D2000 matrix with the epoxy-bifunctional nanofiller CyH-POSS-DGEBA-oligomer (DGEBA replacement, see scheme in Fig. 12, top right). The latter POSS compound proved itself as an efficient stiffening agent for epoxy resins. In Fig. 12 nanocomposites with very similar weight loads of CyH-POSS-DGEBA-oligomer (25 wt%, 33 mol%) and "Sn2" (20 wt%, 10 mol%) are compared after normal cure, after annealing under argon (12 h at 180 °C), and after oxidation treatment (12 h in circulating air at 180 °C).

After normal cure CpPOSS-DGEBA, strongly reinforces the matrix, mainly by physical crosslinking (increase in rubber modulus via POSS-POSS interactions and nano-aggregation), and both POSS and Sn2 slightly raise the T_g. Sn2 is not as an efficient physical crosslinker like CpPOSS-DGEBA and it causes a reduction of the crosslink density, thus leading to a moderately decreased rubber modulus.

After annealing under argon, both the compared nanocomposites experience thermal degradation of the matrix. The POSS nanocomposite does not experience any additional effects, and its storage modulus in the rubber region decreases significantly in comparison to the normally cured state. The mechanical properties of the Sn2 nanocomposite remain nearly unchanged after the annealing: matrix degradation is outbalanced by Sn2 polymerization. Nevertheless, the POSS nanocomposite still displays higher moduli in the rubber region.

After the oxidation treatment, the mechanical properties of the POSS nanocomposite markedly deteriorate, but much less than in the case of the neat matrix. In contrast to this, Sn2 causes a strong reinforcement via oxidative crosslinking.

The above comparison shows, that the POSS nanofillers can cause a stronger mechanical reinforcement via physical

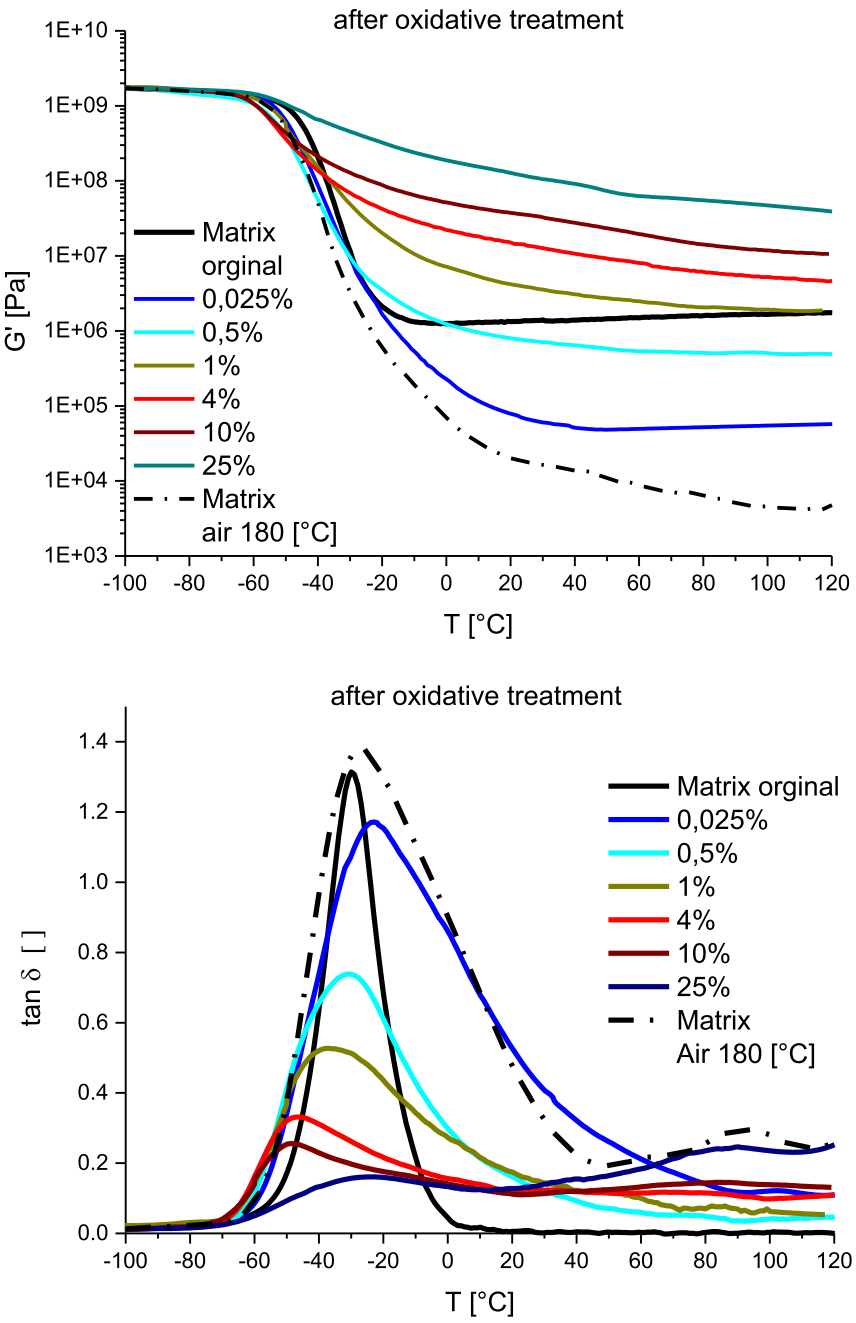

Fig. 11. Effect of nanofiller content on the thermo-mechanical properties of the epoxy-Sn2 nanocomposites which underwent oxidation treatment: Shear storage modulus *G'* (top) and loss factor tan(δ) (bottom) as function of temperature: nanofiller content is in the range of 0.025–25 mol% amino protons.

crosslinking, because they can easily be obtained with strongly crystallizing substituents. During the annealing and oxidation treatment, the POSS seems to hinder the degradation reactions by limiting segmental mobility [26,27] in the matrix. In contrast to this, the butylstannoxane cages are poor physical crosslinkers, but they counteract thermal and oxidative matrix degradation via cage polymerization and via highly efficient oxidative crosslinking reactions.

3.5. Comparison of Sn2 with the previously studied stannoxane cages

In Fig. 13, the anti-oxidative effect of the studied "Sn2" cage is compared with the effect of the previously studied [40] four-aromatic-amino-H-functional stannoxane cage "Sn4", as well as with the effect of the non-functional "Sn0" which was to a small extent (one sample) also studied in Ref. [40], as well as in the authors' later work (publication in preparation). Both Sn4 and Sn0 differ from Sn2 only in the functionality of their sulfonate substituents.

At high filler concentrations, around 20 wt% (see Fig. 13a), the highest matrix stabilization by oxidative crosslinking is achieved by Sn4, a somewhat smaller one by Sn2, and a distinctly smaller one by Sn0, after the oxidation treatment. The neat matrix nearly degrades to a liquid under the test conditions (Fig. 13). The strongest effect of Sn4 can be explained by its highest chemical functionality prior to oxidation. Sn0, in addition to its lowest (zero) functionality also displays a marked micro-phase separation under formation of

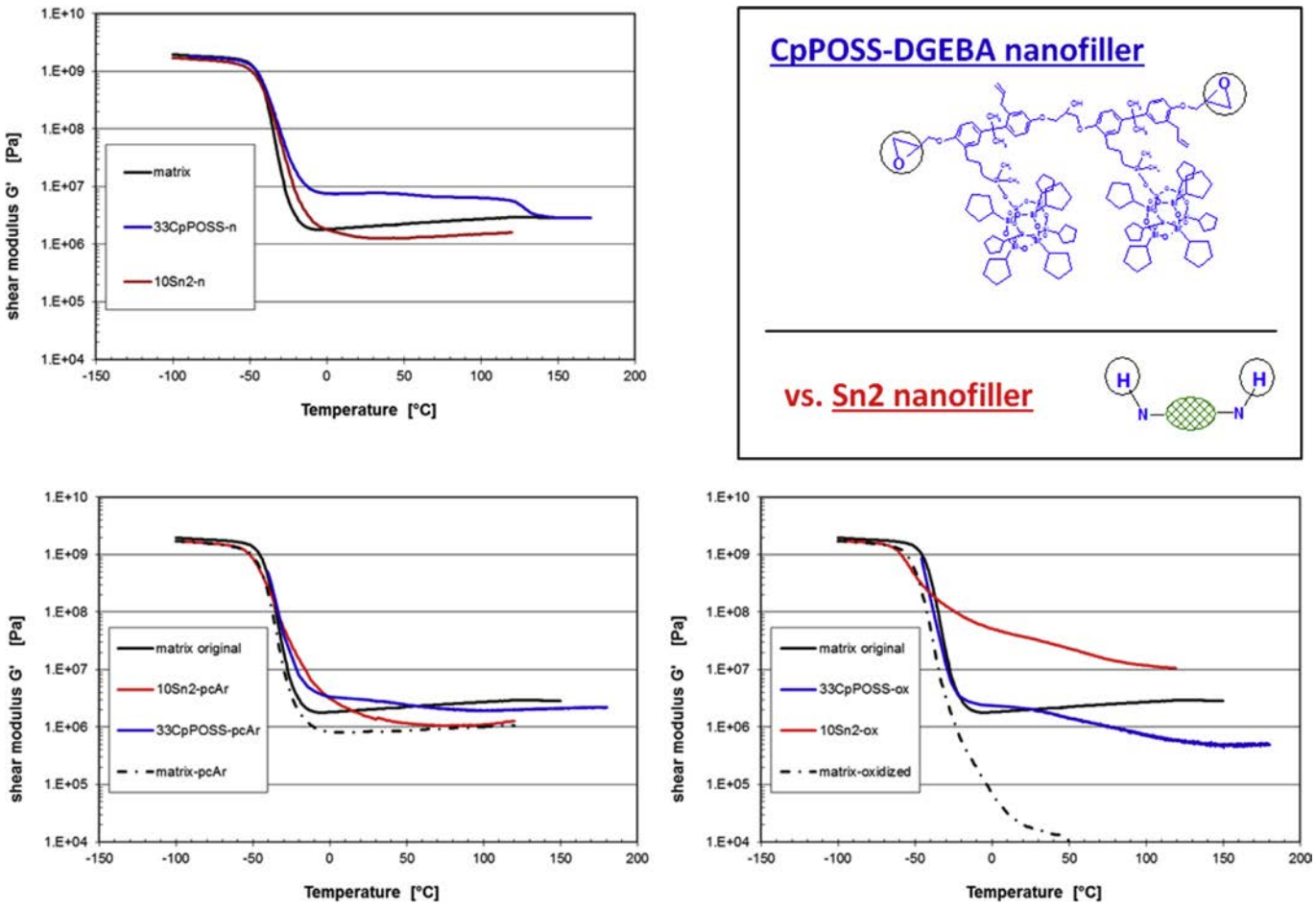

Fig. 12. Comparison of the effect of 25 wt% (33 epoxy-mol %) of the CpPOSS-DGEBA (scheme top right) and of the comparable amount of 20 wt% (10 amino-H-mol %) of Sn2 nanofiller in the DGEBA-D2000 epoxy matrix in different situations: after normal cure (top left), after post-cure under argon (bottom left) and after oxidation treatment (bottom right).

crystallites as reported in Ref. [40], and hence its contact surface with the matrix is highly reduced.

At low filler concentrations, the anti-oxidative efficiency of the cages changes (see Fig. 13b): The most efficient is the Sn2 cage, followed by Sn0 (which is better dispersed at low concentrations) and finally by the branching Sn4 cage. For a comparable stabilizing effect, 7 wt% of Sn4, or 4 wt% of Sn0 or 2 wt% of Sn2 are needed. Sn4 is much less efficient at lower concentrations [40], e.g. at 4 wt% the oxidative degradation already outweighs the oxidative cross-linking. In contrast to this, Sn2 strongly hinders the oxidative degradation even at very low concentrations (see Fig. 11). The reason for the highest anti-oxidative effect of Sn2 seems to be its linear bonding and hence better accessibility for chemical reactions (in contrast to branching Sn4), the nano-aggregation of Sn4 reported in Ref. [40], as well as the tendency of Sn0 to crystallize from the matrix even at low concentrations.

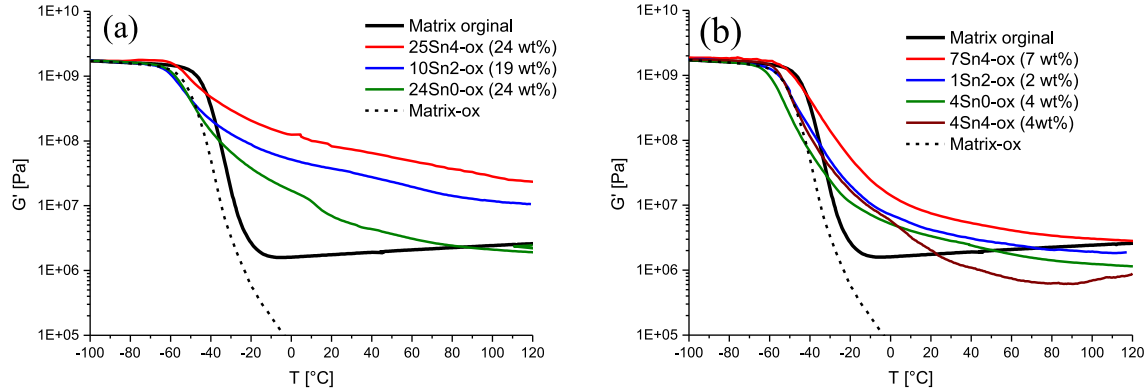

Fig. 13. Comparison of the anti-oxidative effect of Sn2 cages in the DGEBA-D2000 matrix with the effect of previously studied [40] Sn4 and Sn0, the latter of which was further studied in a work which is being prepared for publication; $G = f(T)$ at (a) high filler concentrations around 20 wt%; (b) at low filler concentrations.

4. Conclusions

- The investigated amino-functional stannoxane nanofiller, which can be regarded as a heavier analogue of POSS, displays a high reactivity towards epoxides, which makes possible its rapid and smooth incorporation in epoxy resins, and also a very fine dispersion at low concentrations.
- The good nanofiller dispersion leads to simple effects in the DMTA profiles of the nanocomposites: increase in the glass transition temperature due to the incorporation of heavy and rigid linear building blocks into the polymer, as well as the decrease of the equilibrium rubber modulus at higher nanofiller concentrations, because the bifunctional stannoxane replaces a tetrafunctional amine.
- In contrast to its lighter POSS homologue, the stannoxane cage displays a relatively high chemical reactivity at moderately elevated temperatures. The incorporation as linearly bonded and finely dispersed units highly supports this reactivity.
- The oxidative crosslinking reactions of the stannoxane nanofiller with the epoxy matrix lead to a visible anti-oxidative effect already at concentrations as low as 0.05 wt% (0.025 amino-H%) and to a strong one at 1 wt%. This fact, together with practical unextractability from the nanocomposite, makes the "Sn2" stannoxane a potentially very attractive additive.
- At elevated temperatures in absence of air, the linearly bonded — and under normal conditions practically unextractable — stannoxane displays an unusual short-range mobility in the matrix, which makes possible nano-phase separation under formation of elongated polymeric stannoxane domains (sized typically 15 × 80 nm), much larger than the original nanofiller cages (2.3 × 4.7 nm). This unusual effect is a consequence of the ionic (oxonium) bonding between the nanofiller cage and its function-bearing substituents. This mobility and phase separation is practically not observed during heating in air: The oxidative crosslinking reactions fix the stannoxane cages covalently to the matrix and prevent their movement.

Acknowledgement

The authors thank Ms. Dana Kaňková for recording NMR spectra, Ms. Miroslava Brunclíková (ATR-FTIR), Ms. Jiřina Hromádková (electron microscopy), Ms. Eva Miškovská (X-ray scattering), and Ms. Zuzana Walterová and Ms. Zuzana Kálalová for the determination of the tin content via ash analysis.

The authors thank Czech Science Foundation, grant Nr. 108/11/2151 for the financial support of this work.

References

[1] Jang J, Bae J, Lee K. Polymer 2005;46:3677–84.
[2] Hakimelahi HR, Hu L, Rupp BB, Coleman MR. Polymer 2010;51:2494–502.
[3] Spirkova M, Brus J, Hlavata D, Kamisova H, Matejka L, Strachota A. Surf Coating Int B Coating Trans 2003;86:187–93.
[4] Zhou Weidong, Yu Yingchao, Chen Hao, DiSalvo FJ, Abruna HD. J Am Chem Soc 2013;135:16736–43.
[5] Matteucci S, Van Wagner E, Freeman BD, Swinnea S, Sakaguchi T, Masuda T. Macromolecules 2007;40:3337–47.
[6] Weng CJ, Huang JY, Huang KY, Jhuo YS, Tsai MH, Yeh JM. Electrochim Acta 2010;55:8430–8.
[7] Lin Z, Cheng YR, Lu H, Zhang LA, Yang B. Polymer 2010;51:5424–31.
[8] Miniewicz A, Girones J, Karpinski P, Mossety-Leszczak B, Galina H, Dutkiewicz M. J Mater Chem C 2014;2:432–40.
[9] Kuila BK, Park K, Dai LM. Macromolecules 2010;43:6699–705.
[10] Hu GJ, Zhao CG, Zhang SM, Yang MS, Wang ZG. Polymer 2006;47:480–8.
[11] Kim H, Abdala AA, Macosko CW. Macromolecules 2010;43:6515–30.
[12] Dai YL, Xiao HH, Liu JH, Yuan QH, Ma PA, Yang DM, et al. J Am Chem Soc 2013;135:18920–9.
[13] Horak D, Trchova M, Benes MJ, Veverka M, Pollert E. Polymer 2010;51:3116–22.
[14] Wu JR, Huang GS, Li H, Wu SD, Liu YF, Zheng J. Polymer 2013;54:1930–7.
[15] Maji PK, Das NK, Bhowmick AK. Polymer 2010;51:1100–10.
[16] Spirkova M, Strachota A, Urbanova M, Baldrian J, Brus J, Slouf M, et al. Mater Manuf Process 2009;24:1185–9.
[17] Spirkova M, Brus J, Brozova L, Strachota A, Baldrian J, Urbanova M, et al. Prog Org Coat 2008;61:145–55.
[18] Dal Pont K, Gérard J-F, Espuche E. J Polym Sci Part B Polym Phys 2013;51:1051–9.
[19] Xu Z, Gao C. Macromolecules 2010;43:6716–23.
[20] Fukumaru T, Fujigaya T, Nakashima N. Macromolecules 2013;46:4034–40.
[21] Milliman HW, Ishida H, Schiraldi DA. Macromolecules 2012;45:4650–7.
[22] Spirkova M, Strachota A, Strachotova B, Urbanova M. Surf Eng 2008;24:268–71.
[23] Oleksy M, Galina H. Ind Eng Chem Res 2013;52:6713–21.
[24] Matějka L, Strachota A, Pleštil J, Whelan P, Steinhart M, Šlouf M. Macromolecules 2004;37:9449–56.
[25] Strachota A, Kroutilová I, Kovářová J, Matějka L. Macromolecules 2004;37:9457–64.
[26] Strachota A, Whelan P, Kříž J, Brus J, Urbanová M, Šlouf M, et al. Polymer 2007;48:3041–58.
[27] Brus J, Urbanova M, Strachota A. Macromolecules 2008;41:372–86.
[28] Eychenne-Baron C, Ribot F, Steunou N, Sanchez C. Organometallics 2000;19:1940–9.
[29] Ribot F, Escax V, Martins JC, Biesemans M, Ghys L, Verbruggen I, et al. Chem Eur J 2004;10:1747–51.
[30] Van Lokeren L, Willem R, van der Beek D, Davidson P, Morris GA, Ribot F. J Phys Chem C 2010;114:16087–91.
[31] Puff H, Reuter H. J Org Chem 1989;373:173–8.
[32] Dakternieks D, Zhu H, Tiekink ERT, Colton RJ. J Organomet Chem 1994;476:33–8.
[33] Chandrasekhar V, Gopal K, Singh P, Narayanan RS, Duthie A. Organometallics 2009;28:4593–601.
[34] Holmes RR. Acc Chem Res 1989;22:190–4.
[35] Ribot F. In: Davies AG, Gielen M, Pannell KH, Tiekink ERT, editors. Tin chemistry: fundamentals, frontiers, and applications. Chichester (UK): Wiley; 2008. pp. 69–92.
[36] Eychenne-Baron C, Ribot F, Steunou N, Sanchez C. J Organomet Chem 1998;567:137–42.
[37] Ribot F, Banse F, Diter F, Sanchez C. New J Chem 1995;19:1145–53.
[38] Ribot F, Lafuma A, Eychenne-Baron C, Sanchez C. Adv Mater 2002;14:1496–9.
[39] Ribot F, Veautier D, Guillaudeu SJ, Lalot T. J Mater Chem 2005;15:3973–8.
[40] Strachota A, Ribot F, Matějka L, Whelan P, Starovoytova L, Plestil J, et al. Macromolecules 2012;45:221–37.